Journal Pre-proof

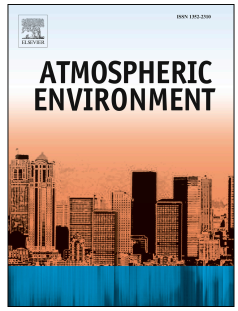

Insight into the climatology of different sand-dust aerosol types over the Taklimakan Desert based on the observations from radiosonde and A-train satellites

Honglin Pan, Wen Huo, Minzhong Wang, Jiantao Zhang, Lu Meng, Kanike Raghavendra Kumar, N.S.M.P. Latha Devi

PII: S1352-2310(20)30437-4

DOI: https://doi.org/10.1016/j.atmosenv.2020.117705

Reference: AEA 117705

To appear in: *Atmospheric Environment*

Received Date: 2 January 2020

Revised Date: 7 June 2020

Accepted Date: 11 June 2020

Please cite this article as: Pan, H., Huo, W., Wang, M., Zhang, J., Meng, L., Kumar, K.R., Devi, N.S.M.P.L., Insight into the climatology of different sand-dust aerosol types over the Taklimakan Desert based on the observations from radiosonde and A-train satellites, *Atmospheric Environment* (2020), doi: https://doi.org/10.1016/j.atmosenv.2020.117705.

CRediT authorship contribution statement:

Honglin Pan: Conceptualization, Formal analysis, Investigation, Data curation, Visualization, Writing-original draft preparation. **Wen Hou:** Conceptualization, Supervision, Resources, Writing-review and editing. **Minzhong Wang:** Conceptualization, Supervision, Project administration, Funding acquisition, Writing-review and editing. **Jiantao Zhang:** Formal analysis, Investigation, Data curation. **Lu Meng:** Visualization, Data curation. **Kanike Raghavendra Kumar:** Formal analysis, Investigation, Writing-review and editing. **N.S.M.P. Latha Devi:** Data curation, Language editing and formatting. All authors have read and agreed to the published version of the manuscript.

Graphical Abstract

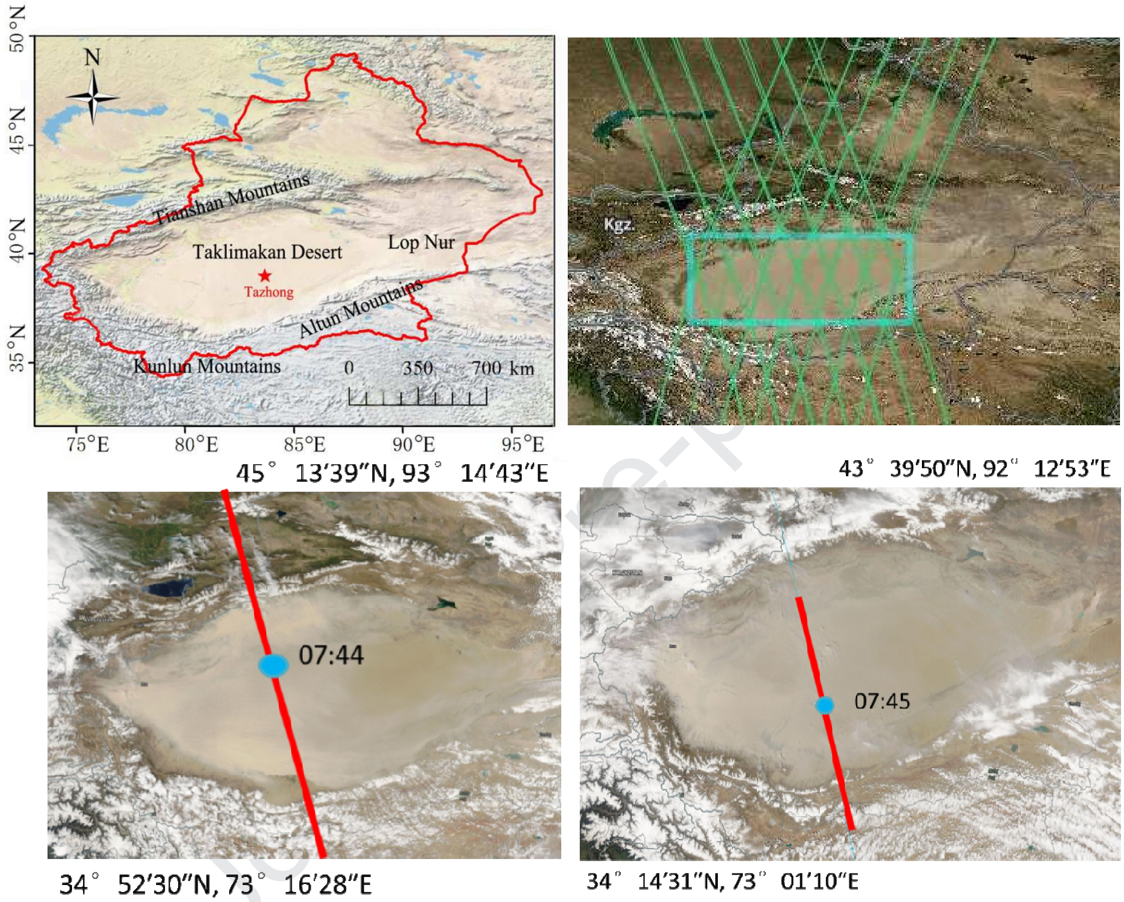

Insight into the climatology of different sand-dust aerosol types over the Taklimakan Desert based on the observations from radiosonde and A-train satellites

Honglin Pan[a], Wen Huo[a,*], Minzhong Wang[a,**], Jiantao Zhang[a], Lu Meng[a], Kanike Raghavendra Kumar[b,c], N.S.M.P. Latha Devi[b]

[a]*Taklimakan Desert Meteorology Field Experiment Station of CMA, Institute of Desert Meteorology, China Meteorological Administration (CMA), Urumqi 830002, Xinjiang, China*

[b]*Department of Physics, Koneru Lakshmaiah Education Foundation (KLEF), Vaddeswaram 522502, Guntur, Andhra Pradesh, India*

[c]*Collaborative Innovation Centre on Forecast and Evaluation of Meteorological Disasters, Key Laboratory of Meteorological Disaster, Ministry of Education (KLME), Key Laboratory of Aerosol-Cloud-Precipitation of China Meteorological Administration, School of Atmospheric Physics, Nanjing University of Information Science and Technology, Nanjing 210044, Jiangsu, China*

.

<u>*Corresponding author(s)</u>

Email: huowenpet@idm.cn (W. Huo); wangmz@idm.cn (M. Wang)

Abstract

The vertical distributions of sand-dust aerosols (SDAs) over the Taklimakan Desert (TD; 37°N–41°N, 78°E–88°E) that occurred during the spring are essential for both long-range transport and climate effects, apart from the living environment and health. In this study, we investigated the optical properties of SDAs and evaluated the correlation between optical properties and meteorological factors over the TD area located in the northwest of China. For this, we have utilized the A-train multiple-satellite remote sensing data provided quasi-synchronized observations by the Cloud-aerosol Lidar and Infrared Pathfinder Satellite Observations (CALIPSO), CloudSat, and Moderate Resolution Imaging Spectroradiometer (MODIS) instruments for the study period during 2007-2010. Besides, we have verified the meteorological factors observed from the CALIPSO to know the applicability and reliability with the Radiosonde sounding data. We found that the cloud–aerosol discrimination (CAD) algorithm can accurately identify clouds and SDAs over the TD area, especially during blowing dust/floating dust (BD/FD). Overall, it is revealed that the total depolarization ratio of SDAs is below 0.5. Besides, the temperature (T) and pressure (P) of CALIPSO satellite products data are in excellent agreement with the radiosonde sounding measured data over the TD area. Further, most data points during the DS (BD/FD) event spread towards lower (higher) relative humidity (RH) ranged between 0.0386 and 0.6306 (0.1079 and 1.00). Our analysis provides the observational evidence from the CALIOP that the optical properties of vertical dust particles and

meteorological elements over the TD have distinct variability below and above 4 km height for DS and BD/FD events. The results obtained will provide not only reliable reference values for the improvement of the CAD algorithm used in the CALIPSO but also provide critical information for model evaluation and enhancement of CALIPSO products.

***Keywords**:* CALIPSO; CloudSat; Sand-dust aerosol; Radiosonde; Taklimakan Desert.

1. Introduction

Sand-dust aerosols (SDAs), one of the essential aerosol types (i.e., mineral dust particles mainly from the desert), affect the energy balance and the hydrological cycle. They induce directly by absorbing and scattering of solar radiation and indirectly by altering cloud microphysical properties (Twomey et al., 1984; Chen et al., 2017), causing air pollution and thus posing health hazards for humans (Tanaka and Chiba, 2006; Nan and Wang, 2018). The Taklimakan Desert (TD), the second-largest desert in the world, extends between 37°N–41°N and 78°E–88°E (Fig. 1) located in the central Tarim Basin, Xinjiang and the hinterland of the Eurasian continent in the mid-latitude region of the Northern Hemisphere (Wang et al., 2016; Pan et al., 2019). It is surrounded by the Lake Lop Nur (which is a salt lake), the Kunlun Mountains, the Pamir Plateau, and the Tianshan Mountains in the east, south, west, and north directions, respectively, forming a unique terrain surrounded by the mountains on three sides and a depression on one side (Sun et al., 2001; Lu et al., 2018). Because of the Qinghai–Tibet Plateau and its surrounding mountainous areas block the transport of ocean water vapor, the TD region has become an extremely arid climate area with dry winters and little rain in summer. It has the characteristics of sufficient thermal conditions, scarce precipitation, intense sunshine, the significant temperature difference between day and night, and sparse desert vegetation, which constitutes a unique and extremely fragile natural ecosystem. The desert has a very different climate and underlying surface conditions to those in other parts of the world. Its atmospheric boundary layer structure and land surface processes are unique and have significant influences on the regional climate and atmospheric circulation (Yumimoto et al., 2009; Ge et al., 2016).

The TD area provided the most substantial contribution to global dust emissions, next to the Sahara Desert in Africa (Ma et al., 2013; Mehta et al., 2018). Previous studies have found that dust particles from the TD can fertilize not only the Pacific Ocean but also the North Atlantic Ocean (Yumimoto et al., 2009). These particles also contribute to background dust in the free atmosphere and affect the radiative budget at high altitudes through scattering and absorption. During its extraordinary long-range transport, the dust even reaches heights where it could create nucleation sites for ice clouds (Sakai et al., 2004; Sassen et al., 2003). Also, Huang et al. (2009) found that dust aerosols have a significant impact on the radiative energy budget over the TD, which can heat the atmosphere between 1 and 3 K day^{-1}. The altitudes of Asian dust loading in the atmosphere are essential for both long-range transport and climate effects. The case studies showed that the dust particles from the TD could reach the upper troposphere from 4 to 10 km above sea level by strong convective updrafts, and then be transported more than one full circuit around the globe in about 13 days (Eguchi et al., 2009; Groussetet al., 2003; Uno et al., 2009). Eguchi et al. (2009) found a two-layered dust vertical distribution over the northeastern Pacific and North America in May 2007. The upper dust cloud (4–10 km) was seen above the primary cloud layer and mainly originated from the dust storms (DSs) that occurred over the TD, and probably unmixed with the Asian pollutants. Whereas the lower dust layer (0–4 km) was largely generated from the DS that occurred in the Gobi Desert and got mixed with anthropogenic aerosols.

Besides, the radiative effects of Asian dust are significantly determined by the vertical distributions (Huang et al., 2014). However, the net SDA climate effects (direct, indirect, and semi-direct) are still highly uncertain. The model simulations of aerosol vertical distributions differ by up to one order of magnitude, leading to significant uncertainties in climate effects (e.g., Textor et al., 2006; Rosenfeld et al., 2008; Guo et al., 2016). The impact of DSs over the TD area on the radiative energy budget and the implications for the regional climate are open questions (Huang et al., 2009; Shao et al., 2013; Yang et al., 2019；Zhang et al., 2019). Besides, due to unique topography, the Taklimakan dust lower than 5 km cannot be easily transported out of this desert (Ge et al., 2014). Still, it can be entrained in height between 5 km and 10 km and carried horizontally over long distances by the westerlies during the DSs (Yumimoto et al., 2009), even on a global scale from Asia to North America (Shao et al., 2013; Zhang et al., 2019). The atmospheric dust has been observed across the continents and oceans, giving rise to its importance in both terrestrial and marine ecosystems (Huebert et al., 2003; Mahowald et al., 2009; Kok et al., 2017). Furthermore, many studies have been utilizing the CALIPSO data to analyze SDAs in different areas and helping to develop the accuracy of CAD algorithm (Tian et al., 2017; Vaughan et al., 2019; Benkhalifa et al., 2019; Bozlaker et al., 2019; Luo et al., 2020; Zeng et al., 2020).

The Cloud-Aerosol Lidar observed the detection of dust weather signals and more accurate discrimination between clouds and SDA with Orthogonal Polarization (CALIOP) sensor aboard the Cloud-aerosol Lidar and Infrared Pathfinder Satellite Observations (CALIPSO) satellite. It is critical to retrieve the cloud and aerosol optical properties with more precise and high accuracy. Seasonally, the DSs over East Asia occurred and were more active primarily during the spring season. Few studies have provided more accurate results and evaluated the ability of CALIPSO detection under different intensities of sand-dust weather and discrimination between clouds and SDA using the version 4.2 algorithms. Further, the discussion on the vertical distribution characteristics of SDA was also provided under different intensities of sand-dust weather conditions. Also, the variation characteristics of atmospheric conditions under different sand-dust weather conditions utilizing the radiosonde data is required and could be studied to verify the CALIOP data.

In this study, we examined the vertical distributions of DS particles over the TD and downwind regions using the satellite observations for typical cases of sand-dust weather conditions. This task is undertaken here to verify the efficiency and accuracy of the CALIPSO datasets applied over the TD region and the vertical distribution of dust aerosols and associated atmospheric conditions under different intensities of dust weather (including floating dust (FD), blowing dust (BD), and dust storm (DS)) during spring over the study domain. This work not only provides a reference and assessment of applicability for the use of CALIPSO products in the analysis of SDAs under different intensities of dust weather during spring over the TD region but also facilitates improvements to the CALIPSO datasets over this region and provides critical information for model evaluations and validation, where there are sparse observations.

2. Data and methods

2.1. Satellite data

2.1.1. The CALIPSO

The CALIPSO satellite was launched on April 28, 2006, to study the role of clouds and aerosols in climate and weather (Winker et al., 2007; Zhang et al., 2018; Pan et al., 2019). The LIght Detection And Ranging (LIDAR) is a powerful remote sensing technique for obtaining information related to the vertical distribution of aerosols in the atmosphere (Liu et al., 2002). On a global scale, the lidar data are acquired by the CALIOP, which is a primary instrument aboard the CALIPSO satellite (Winker et al., 2007). The CALIPSO developed as a collaboration project between NASA, and the space agency of France (CNES) has provided altitude-resolved profiles of aerosols and clouds, since June 2006 (Winker et al., 2009). The CALIOP provides global and continuous information on the vertical distribution of aerosols and clouds. In addition to the total attenuated backscatter signal obtained at two wavelengths (532 nm and 1064 nm), the CALIOP is capable of acquiring polarization measurements at 532 nm. As the particle depolarization ratio is considered as the fingerprint of desert dust particles (Ansmann et al., 2003; Liu et al., 2008), the CALIOP is an ideal instrument for studies related to the three-dimensional distribution and transport of dust in the atmosphere (Amiridis et al., 2013; Proestakis et al., 2018). At present, the researchers around the world utilized the CALIPSO products to a greater extent to understand the impact of aerosols and clouds on the Earth's radiation budget (Kumar et al., 2018; Pan et al., 2019). The CALIPSO/CALIOP (version 4.10) aerosol products used in this study are:

(i) Level-1B products (temporal resolution: 0.05 s, vertical and spatial resolution: 30 m (0-8.2 km) and 333 m), include Total_Attenuated_Backscatter_532/Attenuated Depolarization Ratio/Attenuated Color Ratio.

(ii) Level-2 products: Aerosol profile (temporal resolution: 5.92 s, vertical and spatial resolution: 60m×5km), include Extinction_Coefficient_532/

Particulate_Depolarization_Ratio_Profile_532/Temperature/Pressure/Relative_Humidity/Column_Optical_Depth_Tropospheric_Aerosols_532.

(iii) Vertical feature mask (VFM) product (temporal resolution: 0.74 s, vertical and horizontal resolution: 30 m (-0.5 to 8.2 km) and 333 m, 60m (8.2 to 20.2 km) and 1000 m. Include Feature_Classification_Flags (feature type/cloud type/aerosol type).

2.1.2. The CloudSat instrument

The CloudSat equipped with 94 GHz CPR (Cloud Profile Radar, W-band) is the first solar polar-orbiting satellite dedicated to observing clouds with the characteristic of high vertical resolution. It can be used to probe the three-dimensional structure of clouds globally (Stephens et al., 2008). The satellite is located on a solar synchronous orbit at the height of around 705 km, and a satellite that orbits the Earth in one complete circle is called a scan track. The total orbit time and length are about 99 min and 40,022 km, respectively. Each rail has 36,383 sub-satellite pixel points, a beam coverage width with an along-rail resolution of 2.5 km, and a cross-rail resolution of 1.4 km, together with a vertical resolution of 240 m at each sub-satellite pixel point. The CloudSat not only focuses on the detection of cloud layers consisting of larger-scale particles with higher optical thickness but on the internal information of clouds. It can generate a vertical profile from the liquid and frozen water content in the cloud. Still, it is not detailed enough to probe thin clouds at the top, and therefore, difficult to present information on the aerosol distribution (Pan et al., 2017).

The CloudSat cloud products used in this study are:

(i) 2B-GEOPROF, include Radar_Reflectivity: Radar Reflectivity Factor; CPR_Cloud_mask: CPR Cloud Mask.

(ii) 2B-CLDCLASS-LIDAR, include Cloud Layer Base; Cloud Layer Top; Cloud Layer Type. The data products were processed combined in radar-only and lidar-only as well as a radar-lidar mode with the CALIPSO or moderate-resolution imaging spectroradiometer (MODIS) data.

These two sensors have led to the development of many retrieval algorithms and greatly improved our knowledge on cirrus/ice cloud distributions and its characterization as well as the classification of clouds and aerosols (Mace et al., 2009; Pan et al., 2017, 2019; Mehta et al., 2018; Kumar et al., 2018). However, few studies have utilized both sensors to analyze and evaluate aerosol detection, and useful classification of clouds and aerosols.

2.1.3. The MODIS sensor

The MODIS onboard Terra and Aqua satellites were launched by NASA from 2000 and 2002, respectively. The Aqua satellite, also, is the part of A-train satellite constellations, flying ahead of the CloudSat and CALIPSO only with 45 s and 75 s, respectively. Consequently, the present study utilized the MODIS Aqua satellite to retrieve the true color images used for the validation with the DS outbreak cases by the CALIPSO derived features during the selected days typically representing the optical and physical properties of DS and BD/FD over the study region.

2.2. Meteorological data observed from the Radiosonde

To gain more accurate and comprehensive knowledge of the variations and characteristics of atmospheric conditions under different sand-dust weather conditions, we utilized intensively observed radiosonde meteorological data (hereafter, radiosonde data) to verify some of the data provided by the CALIOP. The radiosonde data used for the assessment is collected at Tazhong (39.04°N, 83.64°E, 1109 m) during the period July 1–30, 2016. Tazhong is located in the hinterland of the TD area, which is shown with a star mark in Fig. 1. The annual averaged temperature in this area was 12.1 °C, with the extreme maximum temperatures varied between 40.0 °C and 46.0 °C. Whereas, the mean yearly precipitation was measured less than 30 mm, and the annual averaged evaporation potential was as high as 3800 mm. However, the winds prevailed from an easterly direction, with a yearly averaged wind speed of 2.3 m s^{-1}. The majority of occurrences of DS and BD/FD were found during the spring and summer seasons, with an annual averaged occurrence of DS, which is more than 30 days, and the prevailing BD and FD weather conditions were as high as 70 and 100 days, respectively. The radiosonde data observation site is open and has no shelter. The surface is shifted sandy land as well as the underlying surface property in Tazhong, basically representing the surface characteristics of the whole TD region.

The average horizontal drift distance of the GPS sounding observation balloon is ~40 km, and the distance between Tazhong and the TD boundary is more than 100 km. Therefore, after the launch of the sounder, the ground it passes over is desert surface.

The timing of GPS sounding observations is four times a day at 01:15, 07:15, 13:15, and 19:15 (Beijing local time, UTC+8 h). The meteorological data obtained from the experiment mainly include temperature, humidity, pressure, wind speed, and direction of each layer in vertical height. The data used in this paper are original, observed from the ground up to 14 km. In this paper, we have selected the observed data to verify the reliability and applicability of the meteorological elements detected by the CALIPSO, and explored the relationship between the meteorological parameters and the variation characteristics of different intensities of SDA conditions; and the correlation between different SDA optical parameters and meteorological elements.

The screening principle of site data is based on the closest distance between the CALIPSO during scanning time in transit over Tazhong and the radiosonde sounding station in Tazhong (Fig. 2). Because the ground-based radiosonde sounding data and the CALIPSO satellite sounding data are not consistent in space, and hence, included with errors. Also, the maximum deviation distance is limited to 20 km, which means, if the distance between the observation station and the satellite scanning transit position is more than 20 km; hence no data processing is done (Sheng et al., 2003). At the vertical height, the spatial matching is done based on the vertical resolution of 60 m detected by the CALIPSO, and the selected comparison sites are shown in Table 1.

To quantitatively understand the difference between the CALIPSO satellite inversion data and the radiosonde sounding measured data observed from the corresponding stations, this paper provides the calculations of the mean error (ME), mean absolute error (MAE), root mean square error (RMSE), and correlation coefficient (R) (Jolliffe and Stephenson, 2011).

3. Results and discussion

3.1. Dust events over the TD – A case study

Dust events are defined as the observations of floating dust (FD), blowing dust (BD), and dust storm (DS) (Huang et al., 2008). As satellite data products do not clearly define and distinguish between FD and BD, and the gap between the two is small, and hence, the present study does not subdivide FD and BD, just defined the DS and BD/FD only. Based on our previous investigation (Pan et al., 2019), we found that: the dust events in TD area mainly occurred during the spring and summer seasons, and the annually-averaged probability ratio of different dust events is as follows: FD (56.75%), BD (35.84%), DS (7.41%). To better identify the sandstorm, this paper combines the CALIPSO, CloudSat, and Aqua MODIS quasi synchronous joint detection data. While the CALIPSO and CloudSat joint detection data only provide the detection results for the entire years from 2007 to 2010, and hence, we selected the most typical DS and non-DS events to fully illustrate their characteristics and differences over the domain (Deng et al., 2013).

3.1.1. Dust storm (DS) events

Two typical DS cases were chosen to analyze the optical properties of DS particles, and the ability of CALIPSO to detect them, which are found on April 22, 2007, and April 14, 2010, are presented in Fig. 3. Fig. 3 shows the two DSs outbreaks over the TD area and the locations where the MODIS Aqua overpasses along the orbit track across the TD at 07:44 (Fig. 3a) and 07:45 (Fig. 3b) UTC. These data were acquired on the daytime side of an orbit, as depicted by the CALIOP. On April 22, 2007, the time of CALIPSO overpasses the TD area was around 07:44:21–07:45:26 UTC (Lat: 37.50–40.50 °N, Lon: 83.67–82.74 °E), and the overpass time of CALIPSO on April 14, 2010, was between 07:45:55 and 07:47:02 (Lat: 37.50–40.50 °N, Lon: 83.74–82.81 °E). It can be seen that the location of the DS outbreak is very close to Tazhong.

Fig. 4 shows the CALIPSO and CloudSat (hereafter, 2C) derived features for two typical DS cases observed over the TD. The radar reflectivity observed from the CloudSat 2B-GEOPROF product is shown in Fig. 4A, which illustrates that there is a small cloud at the height of ~6.5 km around 37.5°N. Whereas, Fig. 4B demonstrates clearly that the cloud mask ≥ 30 (yellow) confirms the existence of a cloud at the same height. Fig. 4C presents the cloud information jointly detected by 2C. The results of combined detection are more comprehensive and effective, and we can see that it is As (Altostratus, blue color), where the CloudSat 2B-CLDCLASS-LIDAR product was utilized. In summary, it can be seen that only 'As' clouds were present at the height of ~6.5 km around 37.5°N during the satellite scanning transit when the DS breakout occurred on April 22, 2007.

According to the CALIPSO official website, as mentioned in the summary of the data product guide on Level-1 attenuated backscatter coefficient detection of CALIOP, aerosols were generally shown as yellow/red/orange color. More reliable, strong cloud signals are plotted in gray scales, while weaker cloud returns are similar in strength to strong aerosol returns and coded in yellow and red. Fig. 4D shows the CALIPSO attenuated backscatter measurements demonstrate that at the height of 2-4 km and around 37-41°N, SDA (red-yellow-orange, 0.0015–0.0065 km^{-1} Sr^{-1}) envelops the cloud (gray > 0.0065 km^{-1} Sr^{-1}). Among them, dust particles are the main ones, and clouds (mainly gray-white-colored features) at 2-4 km were also observed by the CALIOP, as shown in Fig. 4E from VFM (Vertical Feature Mask, the CALIPSO VFM 4.10 product which describes the vertical and horizontal types of cloud and aerosol layer, and is used to distinguish dust and cloud). From Figs. 4E-4F, it can be seen that SDA can be lifted to 5 km height. Based on the above analysis, the cloud–aerosol discrimination (CAD) algorithm has identified most SDA features correctly while misidentifying the SDA as a cloud at the height of 2–4 km and around 37–41°N in cyan color. It is notable that “No Signal” is present from the surface up to 1.5 km or 3 km height in Fig. 4E. The misclassifications and “No Signal” happen mainly due to the extremely dense dust when DSs break out occurred, where the lidar signal becomes attenuated (no surface signals are detected), or the thick dust plume has similar optical properties to what would be expected for clouds by the CAD algorithm.

Figs. 4G–H shows the depolarization ratio and attenuated color ratio observed over the study domain. The depolarization ratio is useful for discerning the difference between spherical and non-spherical particles. Non-spherical particles (i.e., dust, ice crystals) change the polarization state of the backscattered light, while spherical particles such as water droplets or spherical aerosols do not. The SDA generally exhibits a depolarization ratio smaller than 0.40 observed at the height of 2–4 km (Fig. 4G). In contrast, the attenuated color ratio can be useful for inferring the information about the size of the particles in the scattering volume. The color ratio will often be smaller than 1 for aerosol layers found at 2–4 km height (Fig. 4H) and greater than 1 for cloud layers depicted at ~10 km height and around 37.5°N (Fig. 4H). This has been confirmed based on the summary of the data product guide and mentioned at https://www-calipso.larc.nasa.gov/resources/calipso_users_guide/browse/index.php.

Furthermore, it can be seen from Fig. 4D, and Fig. 4F that the distribution of dust concentration is uneven when the DSs occurred, and there is a large concentration of dust signal area. At the same time, a typical DS event was also presented in Figs. 4a–h (right panels) occurred on April 14, 2010, and the analysis was found similar to that observed in Figs. 4A–H (left panels).

As stated above, the CloudSat 2B-CLDCLASS-LIDAR product can identify cloud information more effectively and comprehensively. Moreover, the CALIPSO has excellent detection capability for clouds over 5 km. Combined with the detection information of 2C, we noticed that the CAD algorithm of CALIPSO could recognize most of the dust information better. As for the DS events, the CALIPSO misjudges dust as a cloud at a height of 4 km from the surface, and there is a phenomenon of severe signal attenuation. For example, the attenuation range is about 1 km over the TD from the surface to an altitude of 2 km. This revealed that a high concentration of dust particles rose about 1 km from the ground when the DSs occurred. The results of the DS height are consistent with Ming et al. (2009), who utilized the ground-based K_a wavelength millimeter-wave radar to detect the DS height in the TD area during March-May, 2009. Besides, the high values of radar reflectivity (yellow line) located at an elevation below 1 km attributed to the ground surface (combined with Figs. 4E/e), and are consistent with the mean altitude of the TD region as detected by the quasi-synchronized observation of 2C.

3.1.2. Blowing dust/floating dust (BD/FD)

Two typical BD/FD cases of 2C cloud and aerosol discrimination are displayed in Fig. 5. The data were acquired by 2C on May 14, 2007 (without cloud), and May 16, 2008 (with cloud) from nighttime overpass orbit track across the TD region. The products derived from the simultaneous CloudSat radar measurements are presented in Figs. 5A–C and Figs. 5a–c to identify dense clouds and dense dust particles. First, we analyzed the day on May 14, 2007, where the BD/FD particles lifted to ~6 km (Figs. 5A–H). It is depicted that the dust layer is extremely pure without the cloud. Also, a spatially extensive TD dust layer of moderate optical thickness was observed, especially at the height of 6 km, extending from ~37°N to the end at ~41°N. The dust layer is easily identified from the depolarization ratio measurement with green–yellow–orange colors (0.2–0.4), color ratio smaller than 1, and feature type acquired with green at ~6.5 km height (Fig. 5 (left panels)). A relatively dense dust plume (red-gray-colored features in Fig. 5D) is seen between 37° and 38.5°N and below ~5 km, where the lidar signal becomes a little attenuated (black box) and the optical depth, therefore, should be more significant than ~3. Thus, the dense dust plume observed at the height of ~2 km (black box) has been misclassified by the CAD algorithm in Fig. 5E, because its optical properties are similar to what would be expected for clouds.

Meanwhile, we presented another typical case observed on May 16, 2008, with BD/FD lifted to ~12 km (Fig. 5a–h (right panels)). In this scenario, the cloud layer is easily identified which is cirrus observed at the height of 9–12 km (Figs. 5a–d), and surrounded by a low-density dust plume (yellow-colored) lifted to ~12 km (Figs. 5e–h). As it is mentioned before, the color ratio is smaller than 1 for aerosol layers and greater than 1 for cloud layers. However, the cirrus exhibited a depolarization ratio in the range of 0.25–0.40, and those of dust aerosols usually are smaller than 0.40 (Fig. 5g). Furthermore, 2C has detected most cirrus effectively and comprehensively, which is consistent with the reports of Pan et al. (2017). The CALIOP observes the clouds (gray–white-colored features) in Fig. 5d and all clouds in this scene have been identified relatively corrected by the CAD algorithm. We have also noted that, in addition to SDA, the CloudSat radar is also unable to detect optically thin high clouds (e.g., the yellow–orange-colored feature with a white dotted box in Fig. 5d), due to weak detection ability for small particles at radar wavelengths

(3 mm, 94 GHz). A relatively dense dust plume (BD/FD) can be lifted to a height of ~6 km (Fig. 5), while a less thick dust plume (BD/FD) can be raised to relatively higher altitudes (~12 km). Furthermore, the distribution of dust concentration is very uniform when BD/FD events occur. Anyway, as analyzed and studied, the CloudSat and CALIPSO observations together can provide more complete measurements of aerosol and cloud distributions. Moreover, the CAD algorithm can accurately identify clouds and SDA over the TD in BD/FD events, and there are fewer cases of misjudgment.

3.2. Optical properties of SDA

To better estimate the optical properties of SDA and the difference between DS and BD/FD, we deal with the optical parameters of DS and reduce the signal mistakenly judged as the cloud to the signal of SDA, to improve the accuracy and effectiveness of DS information (based on 2C combined products to distinguish dust aerosols and cloud signals, to effectively separate the real clouds or the cases where dust is mistakenly identified as clouds. When the dust aerosol is incorrectly identified as cloud, we delete the so-called cloud signal, and then interpolate it to reduce the impact caused by mistakenly identified). Fig. 6 shows the optical properties of SDA (DS, BD/FD) for four typical cases. The optical depth (OD) for the cases of DS and BD/FD is shown in Fig. 6a. It is evident that the OD of SDA almost exceeds 1.5. During the DS event on April 22, 2007, there were many ODs less than 1.5, because the CAD algorithm mistakenly identified the dust particles as clouds and eliminated the dust information as cloud information, resulting in the discontinuity of OD and hence, resulted in low values. Besides, the CALIPSO cannot detect the DS effectively and comprehensively; and there will be severe signal attenuation at the surface with high dense dust concentration, so the OD obtained by inversion is similar to that of the BD/FD events. Fig. 6b shows the extinction coefficient (EC) for SDA events. The EC of all SDA events increases first and then decreases below 3 km height (dotted line), and the average EC of DS (blue and red lines) is significantly higher than that of BD/FD (yellow and purple lines). The DS in this region could be lifted to ~5 km height, while it could be raised to a higher height attributed to the dynamics of the atmosphere and sand-dust events that frequently occurred during the study period.

Fig. 6c shows the mean depolarization ratio (DR) for SDA events. The mean DR of DS events (red and green) were mainly concentrated at more than 0.4 km and less than 5 km height, and the distribution is relatively scattered. Generally speaking, the mean DR of DS is distributed in the range 0–0.9 and below 6 km. However, this is not the case for BD/FD events. The mean DR of BD/FD events for May 14, 2007 (manganese purple) are mainly concentrated in the range 0.3–0.4 and less than 7 km height; those of the May 16, 2008 events (black) were focused primarily on the range 0.1–0.4 and below 12 km height, with the DR below 7 km decreasing with the height; and the distribution of the mean DR above 7 km is more uniform. It can be seen that there are apparent differences between DS and BD/FD. Also, our results proved once again that SDA generally exhibited a DR smaller than 0.40 (Liu et al., 2009).

However, the mean DR existed at the height of more than 0.4 km and less than 5 km, which implies more presence of non-spherical particles at lower altitudes during the DS outbreak events. Fig. 6d shows the DR for all DS events and BD/FD events. It is revealed that the proportion of DR for DS varied in the range 0.3–0.4 is the largest with 18.75%, while the most substantial percentage (21.89%) of DR for BD/FD found between 0.1 and 0.2. The proportion of DR that occurred in the range of 0-0.3 for the/FD events is higher than that of DS, while the percentage of DR for the DS was found higher in the range 0.3-1.0 than that of BD/FD. In conclusion, the particle DR of DS was mainly occurred in the range 0.2–0.5, while the BD/FD was found primarily on the range of 0.0–0.4. Therefore, the total DR of SDA is mainly concentrated in the range of less than 0.5.

With the above discussion, it is essential to mention here, that firstly the CloudSat and CALIPSO combined products can provide more complete measurements of aerosol and cloud distributions. Moreover, the CAD algorithm can accurately identify clouds and SDA over the TD under most BD or FD events except DS. Secondly, as mentioned in the paper, for DS, the misclassifications and "No Signal" happen mainly due to the extremely dense dust when DS break out occurred, where the lidar (CALIPSO-CALIOP) signal becomes attenuated (no surface signals are detected), or the thick dust plume has similar optical properties to what would be expected for clouds by the CAD algorithm. Thirdly, because dust particles are much smaller than cloud particles, millimeter-wave cloud profile radar (CloudSat-CPR) is not sensitive to detection of dust particles, so millimeter-wave cloud radar cannot effectively detect dust storm particles; because the millimeter-wave cloud radar can effectively detect the cloud signal, the CloudSat and CALIPSO combined products just can only distinguish the cloud and non-cloud signals when the CAD algorithm mistakenly judges dust as a cloud. All in all, further identification of cloud and DS signals needs to be combined with more other detection methods. On the other hand, because of the scarcity of observation stations in the TD, although there is some uncertainty in conclusion, even so, the study of typical cases can play a vital role in the correction of SDAs and cloud process retrieved by satellite remote sensing, which is still very valuable for us to understand further the distribution characteristics of SDAs and cloud in Taklimakan Desert. Later, the authors will devote themselves to further research.

3.3. Variation of meteorological elements with altitude

3.3.1. Applicability of meteorological factors from the CALIPSO

The contour density plots of temperature (T), pressure (P), and relative humidity (RH) distributions obtained between the CALIPSO satellite product and radiosonde observational dataset are used to evaluate the applicability of meteorological parameters over the TD area (Fig. 7). It is revealed that a small dispersion was observed during the study period, represents an increase in T-CALIPSO (temperature obtained from the CALIPSO) with an increase in T-radiosonde (temperature measured from the radiosonde) and the same has been found in P (Figs. 7A and B). Relatively, there is a large dispersion in the data points observed in RH-CALIPSO with RH-radiosonde (Fig. 7C). However, the T data obtained from the CALIPSO are in excellent agreement comparative with the radiosonde sounding data (T_ME=0.3804; T_RMSE=1.6812; T_R=0.9977), which indicates that the T-CALIPSO data is suitable over the hinterland region in the TD area. Similarly, the P-CALIPSO satellite products are almost identical with the P-radiosonde sounding data (P_ME=3.6432; P_RMSE=4.3342; P_R=0.9999), which shows that the applicability of the P data is opted to chose in the desert hinterland. Therefore, the applicability of CALIPSO satellite products' for T and P data is excellent, which can effectively make up for the severe lack of coverage of sounding data in these complex terrain areas. In contrast, there is a large degree of dispersion of RH (RH_ME=0.0124; RH_RMSE=0.2185; RH_R=0.5955), and the RH from the CALIPSO satellite products have relatively low correlation with the RH-radiosonde sounding data due to the time difference of about two hours between the two data sets.

Meanwhile, the mean errors (ME) were analyzed to understand whether the CALIPSO satellite products overestimated or underestimated (Fig. 8). It is revealed that the T of CALIPSO products were slightly overestimated during the study period (Figs. 8A) during most days. However, the trends of MAE and RMSE are consistent in T. It is evident that the RH was slightly underestimated as well as overestimated during the study period (Fig. 8B). Furthermore, the R between RH-CALIPSO and RH-radiosonde was noted with a moderate correlation of 0.5955. It is worth noting that due to the high correlation of pressure, we do not make a detailed analysis here. Besides, it is found that the P data of the CALIPSO satellite products and radiosonde observations have almost precisely coincided. Hence, the deviation analysis of the vertical profiles also has not been done.

The vertical profiles of the ME, MAE, and RMSE for T and RH observed from the CALIPSO satellite products verified against the radiosonde observations are shown in Figs. 8C and 8D. At about 2 km height, the ME, MAE, and RMSE of T have shown the most significant values, while at about 4 km height, they depicted the lowest. The CALIPSO satellite products indeed overestimate it with increasing altitude (> 4 km). Besides, it is evident that the RH is underestimated by the CALIPSO satellite products below 5 km, while it is overestimated above 5 km, and the smallest ME occurs at 4.5 km height. It can be seen that the CALIPSO satellite products had lower MAE at 1 km. It is also observed that the largest RMSE of RH occurred at about 6 km, which might be related to interactions with the troposphere (Smith and Kushner, 2012). Whereas, the smallest RMSE of RH occurred at 1 km, which is near the ground height over the TD region during the study period.

Overall, the T and P data of CALIPSO satellite products are in excellent agreement with the radiosonde data over the TD. Of these, P is the best factor for observation quality found in this study. T has a significant relative deviation in the lower layer and overestimated the actual T at most altitudes. In comparison, the variation of RH is relatively small in the lower layer, and the real RH value was underestimated below 3 km in the lower layer. This may be related to the unique natural properties of the underlying desert surface. Overall, the T and P data of the CALIPSO satellite has excellent applicability over the TD area.

3.3.2. Comparison of meteorological elements observed from CALIPSO in different intensities of SDA

The variations of T, P, and RH from the CALIPSO satellite products with height during the DS and BD/FD events are shown in Fig. 9. For T, it is evident that there is a temperature inversion phenomenon under the weather of BD/FD below 2 km (Fig. 9A). This is because the two weather conditions occur at about 9 pm (UTC), and the desert surface releases a lot of heat. In the case of DS events, the temperature fluctuated (virtual line frame) at the height of 3 km. This may be related to the temperature of the bare desert increases rapidly, and the atmospheric stratification is always in an unstable state during spring, conducive to the formation and development of DS. However, the T between 4 km and 10 km decreases with height, and hence, there are no apparent fluctuations in T with similar changes observed in P (Fig. 9B). For RH (Fig. 9C), the DS events occurred on April 22, 2007(blue) and April 14, 2010 (red), showed an increasing and decreasing trends at the height of 1–3 km (1-3.5 km) and the maximum value of RH appeared at an altitude of 2 km (3 km), which is consistent with the height of mistaking dust for the cloud. This may be one of the reasons that the CAD algorithm mistakenly identifies clouds and aerosols. For the BD/FD event, the RH decreases first and then increases at heights between 1 and

3 km, and the minimum value of RH appears at an altitude of 1.5 km. Overall, the RH during DS and BD/FD events showed opposite trends at a height below 3 km. This means that there is water vapor transport in the vertical direction during the occurrence of DS, and an increase of aerosol content during the process of DS increases the probability of subsequent precipitation, thus increasing the RH of the air.

3.4. Correlation between optical properties and meteorological factors

The contour density plots between the optical properties (extinction coefficient (EC) and depolarization ratio (DR)) of SDAs and meteorological factors (T, RH) observed during the DS and BD/FD events are presented in Fig. 10. The EC of DS is significantly higher than that of BD/FD. It can be seen that the concentration of DS particles is much higher than that of BD/FD, and the value of DR is concentrated in the region of 0.69 (Figs. 10A and 10G). Towards the T and EC, the number of DS data points spread out into areas of high EC and low T suggested increased dominance of dense aerosols attributed to the DS activities near the land surface, while the BD/FD data points spread out into regions of low EC and high T (Figs. 10B and 10H). Moreover, the more extensive temperature distribution range of BD/FD is due to the greater height of dust particles raised by the BD/FD activity, and the signal loss caused by attenuation at an altitude below 3 km when the DS occurs, and the height of dust particles raised is generally lower than 5 km. The distribution difference of DR between DS and BD/FD events is small. However, there are relatively more coarse-mode particles than fine-mode particles when DSs occurred. For the DS events，most data points spread towards lower RH between 0.038 and 0.631, while the BD/FD events have a large number of data points covered towards higher RH between 0.108 and 1.00 (Figs. 10D and 10J). Further, the RH was much lower for the DS event than BD/FD and combined with T. We can see that the height of dust particles for DS was relatively small, which may be an essential reason why dust is mistakenly identified as the cloud (Figs. 10E–F and 10K–L). Overall, the atmospheric conditions during DSs are dry and cold, while those of BD/FD are relatively warm and wet. Therefore, by checking the low-layer T and RH, the misclassified dense dust layers may be identified in the DS cases. In contrast, some other results showed that the DSs usually occurred during dry and hot air conditions over the source regions in the daytime, due to the enhanced convection in a deepened boundary layer in the other areas (Mbourou et al., 1997).

5. Conclusions

In this study, we investigated the optical properties of sand-dust aerosols (SDAs) using A-train multiple-satellite remote sensing data. We evaluated the correlation between optical properties and meteorological factors observed during the spring over the Taklimakan Desert (TD) area (37°N–41°N, 78°E–88°E) situated in the northwest of China. The data presented in this work is derived from the CALIPSO, the CloudSat, and the MODIS instruments for the selected domain during the period between 2007 and 2010. Besides, we have verified the applicability and reliability of the meteorological elements of CALIPSO satellite data products over the TD area using the radiosonde sounding data measured from July 1–30, 2016. The following are the main conclusions established from the results obtained in this study.

1. The CAD algorithm can accurately identify clouds and SDAs over the TD under BD/FD conditions, and there are fewer cases of misjudgment. For DS event, the lidar signal becomes attenuated (no surface signals are detected), and the incredibly thick dust plume could be misclassification as clouds by the CAD algorithm. It is worth noticing that the CAD algorithm works well in most BD/FD cases, but not in the DS.

2. The optical depth of SDAs revealed from the observations is almost more than 1.5. Further, the value of the total particle depolarization ratio (DR) of SDAs is less than 0.5. Moreover, the T and P data of the CALIPSO satellite products are in excellent agreement with the radiosonde sounding data in the TD. Of these, P is the best factor for observation quality in this study. In contrast, T fluctuated notably at the height of 3 km during DS events. Whereas, the RH showed an opposite trend at an altitude below 3 km for the DS and BD/FD events. However, no significant differences were found in P for DS and BD/FD.

3. For DS events, most data points spread towards lower RH between 0.0386 and 0.6306, while BD/FD events have a large number of data points covered towards higher RH between 0.1079 and 1.00. The atmospheric conditions of DSs are dry and cold, while those of BD/FD are relatively warm and wet in the TD. Therefore, by checking the low-layer T and RH, the misclassified dense dust layer may be identified in DS cases. Additionally, many DS data points spread out into regions of high EC,

and low T suggested an increased dominance of dense aerosols attributed to DS activities near the land surface, while BD/FD data points spread out into regions of low EC and high T.

Overall, the results mentioned above will not only help us to understand the optical properties of global SDAs better, and sand-dust emission and transport; but will also provide critical information for model evaluations and improvements in the CALIPSO satellite products. They also offer reliable reference values for the improvement of the CAD algorithm in CALIPSO. Further research on SDAs should focus on combining the CALIPSO measurements with other A-Train satellite measurements, as well as measurements from aircraft and surface network/supersites in the TD area.

Conflicts of interest

The authors declare that they have no conflict of interest. The funders had no role in the design of the study; in the collection, analyses, or interpretation of data; in the writing of the manuscript, or in the decision to publish the results.

CRediT authorship contribution statement:

Honglin Pan: Conceptualization, Formal analysis, Investigation, Data curation, Visualization, Writing-original draft preparation. **Wen Hou:** Conceptualization, Supervision, Resources, Writing-review and editing. **Minzhong Wang:** Conceptualization, Supervision, Project administration, Funding acquisition, Writing-review and editing. **Jiantao Zhang:** Formal analysis, Investigation, Data curation. **Lu Meng:** Visualization, Data curation. **Kanike Raghavendra Kumar:** Formal analysis, Investigation, Writing-review and editing. **N.S.M.P. Latha Devi:** Data curation, Language editing and formatting. All authors have read and agreed to the published version of the manuscript.

Funding Sources

This work was financially supported by the National Natural Science Foundation of China (Grant Nos. 41775030, 41875019, 41575008), and the Flexible Talents Introducing Project of Xinjiang for the years 2017-2018. The authors KRK and NMSPL are grateful to the Department of Science and Technology (DST), Govt. of India, for the award of DST-FIST Level-1 (SR/FST/PS-1/2018/35) scheme to the Department of Physics, KLEF.

Acknowledgments

We are grateful to the CloudSat (http://www.cloudsat.cira.colostate.edu/), the CALIPSO (https://eosweb.larc.nasa.gov/), and the MODIS (https://lance.modaps.eosdis.nasa.gov) instrument scientific teams at NASA for the provision of satellite data, which is available online and formed the central database in the present work. The authors would like to acknowledge Prof. James Jay Schauer, the Editor-in-Chief and Prof. Zhengqiang Li, Associate Editor of the Journal, and the two anonymous reviewers for their helpful comments and constructive suggestions towards the improvement of earlier versions of the manuscript.

References

Amiridis, V., Wandinger, U., Marinou, E., Giannakaki, E., Tsekeri,A., Basart, S., Kazadzis, S., Gkikas, A., Taylor, M., Baldasano,J., and Ansmann, A.: Optimizing CALIPSO Saharan dust retrievals, Atmos. Chem. Phys., 13, 12089–12106. https://doi.org/10.5194/acp-13-12089-2013, 2013.

Ansmann, A., Bösenberg, J., Chaikovsky, A., Comeron, A.,Eckhardt, S., Eixmann, R., Freudenthaler, V., Ginoux, P.,Komguem, L., Linne, H., Lopez Marquez, M. A., Matthias, V.,Mattis, I., Mitev, V., Muller, D., Music, S., Nickovic, S., Pelon, J.,Sauvage, L., Sobolewsky, P., Srivastava, M. K., Stohl, A., Torres,O., Vaughan, G., Wandinger, U., and Wiegner, M.: Long-range transport of Saharan dust to northern Europe: the 11–16 October 2001 outbreak observed with EARLINET, J. Geophys.Res., 108, 4783. https://doi.org/10.1029/2003JD003757,2003.

Benkhalifa, J., J. F. Léon and M. Chaabane, 2019: "Aerosol vertical distribution, optical properties and dust transport in the Western Mediterranean Basin (Case Study: Summer 2012)", *Aerosol Pollution Research,* **10**, 1291-1298, https://doi.org/10.1016/j.apr.2019.02.013.

Bozlaker, A., J. M. Prospero, J. Price and S. Chellam, 2019: "Identifying and Quantifying the Impacts of Advected North African Dust on the Concentration and Composition of Airborne Fine Particulate Matter in Houston and Galveston, Texas", *J. Geophys. Res. Atmos.*, **124**, 12282-12300, https://doi.org/10.1029/2019JD030792.

Chen, S.; Huang, J.; Li, J.; Jia, R.; Jiang, N.; Kang, L.; Ma, X.; Xie, T. Comparison of dust emission, transport, and deposition between the Taklimakan Desert and Gobi Desert from 2007 to 2011. Sci. China Earth Sci. 2017, 60, 1–18.

de Leeuw G., Sogacheva L., Rodriguez E., et al. Two decades of satellite observations of AOD over mainland China using ATSR-2, AATSR and MODIS/Terra: data set evaluation and large-scale patterns. Atmospheric Chemistry and Physics, 2018, 18(3):1573-1592.

Deng M, Mace G G, Wang Z, et al. Evaluation of Several A-Train Ice Cloud Retrieval Products with In Situ Measurements Collected during the SPARTICUS Campaign. Journal of Applied Meteorology and Climatology, 2013, 52(4):1014-1030.

Eguchi, K., Uno, I., Yumimoto, K., Takemura, T., Shimizu, A., Sugimoto, N., et al., 2009.Trans-pacific dust transport: integrated analysis of NASA/CALIPSO and a global aerosol transport model. Atmos. Chem. Phys. 9, 3137–3145.

Field, J. P., Belnap, J., Breshears, D. D., Neff, J. C., Okin, G. S., Whicker, J. J., Painter, T. H., Ravi, S., Reheis, M. C., and Reynolds, R. L.: The ecology of dust, Front. Ecol. Environ., 8, 423–430. https://doi.org/10.1890/090050, 2010.

Ge, J., Huang, J., Xu, C., Qi, Y., Liu, H., 2014. Characteristics of Taklimakan dust emission and distribution: a satellite and reanalysis field perspective. J. Geophys. Res. Atmos. 119.

Ge, J.M., Liu, H., Huang, J., Fu, Q., 2016. Taklimakan Desert nocturnal low-level jet: climatology and dust activity. Atmos. Chem. Phys.16(12), 7773-7783.

Grousset, F.E., Ginoux, P., Bory, A., Biscaye, P.E., 2003.Case study of a Chinese dust plume reaching the French Alps. Geophys. Res. Lett. 30 (10–1).

Guo, J., Deng, M., Lee, S. S., Wang, F., Li, Z., Zhai, P., Liu, H., Lv, W., Yao, W., and Li, X.: Delaying precipitation and lightning by air pollution over the Pearl River Delta. Part I: Observational analyses, J. Geophys. Res.-Atmos., 121, 6472–6488. https://doi.org/10.1002/2015JD023257, 2016a.

Huang J, Minnis P, Chen B, et al. Long□range transport and vertical structure of Asian dust from CALIPSO and surface measurements during PACDEX. Journal of Geophysical Research: Atmospheres, 2008, 113(D23).

Huang, J., Wang, T., Wang, W., Li, Z., Yan, H., 2014.Climate effects of dust aerosols over East Asian arid and semiarid regions. J. Geophys. Res. Atmos. 119.

Huang, J.; Fu, Q.; Su, J.; Tang, Q.; Minnis, P.; Hu, Y.; Yi, Y.; Zhao, Q. Taklimakan dust aerosol radiative heating derived from CALIPSO observations using the Fu-Liou radiation model with CERES constraints. Atmos. Chem. Phys. 2009, 9, 4011–4021.

Huebert, B. J., Bates, T., Russell, P. B., Shi, G., Kim, Y. J., Kawamura,K., Carmichael, G., and Nakajima, T.: An overview of ACE-Asia: Strategies for quantifying the relationships between Asian aerosols and their climatic impacts, J. Geophys. Res., 108, 8633. https://doi.org/10.1029/2003JD003550, 2003.

Huneeus, N., Schulz, M., Balkanski, Y., Griesfeller, J., Prospero, J., Kinne, S., Bauer, S., Boucher, O., Chin, M., Dentener, F., Diehl, T., Easter, R., Fillmore, D., Ghan, S., Ginoux, P., Grini, A., Horowitz, L., Koch, D., Krol, M. C., Landing, W., Liu, X., Mahowald, N., Miller, R., Morcrette, J.-J., Myhre, G., Penner, J., Perlwitz, J., Stier, P., Takemura, T., and Zender, C. S.: Global dust model intercomparison in AeroCom phase I, Atmos. Chem. Phys., 11, 7781–7816. https://doi.org/10.5194/acp-11-7781-2011, 2011.

IPCC (Intergovernmental Panel on Climate Change): Climate change-the physical science basis, Cambridge University Press, New York, 252–271, 2013.

Jolliffe I. T., Stephenson D. B., 2011. Forecast verification: a practitioner’s guide in 494 atmospheric science. Wiley, London, p 292, doi: 10.1002/9781119960003.ch1.

Kok, J. F.: A scaling theory for the size distribution of emitted dust aerosols suggests climate models underestimate the size of the global dust cycle, P. Natl. Acad. Sci. USA, 108, 1016–1021. https://doi.org/10.1073/pnas.1014798108, 2011.

Koren, I., Dagan, G., and Altaratz, O.: From aerosol-limited to in┐ vigoration of warm convective clouds, Science, 344, 1143–1146. https://doi.org/10.1126/science.1252595, 2014.

Kumar A , Singh N , Anshumali, et al. Evaluation and utilization of MODIS and CALIPSO aerosol retrievals over a complex terrain in Himalaya. Remote Sensing of Environment, 2018, 206:139-155.

Kumar K R, Kang N, Yin Y. Classification of key aerosol types and their frequency distributions based on satellite remote sensing data at an industrially polluted city in the Yangtze River Delta, China. International Journal of Climatology, 2018, 38(1): 320-336.

Liu Z, Vaughan M, Winker D, et al. The CALIPSO lidar cloud and aerosol discrimination: Version 2 algorithm and initial assessment of performance[J]. Journal of Atmospheric and Oceanic Technology, 2009, 26(7): 1198-1213.

Liu, D., Wang, Z., Liu, Z., Winker, D., and Trepte, C.: A height resolved global view of dust aerosols from the first year CALIPSOlidar measurements, J. Geophys. Res.-Atmos., 113, D16214. https://doi.org/10.1029/2007JD009776, 2008.

Liu, Z., Sugimoto, N., and Murayama, T.: Extinction-to backscatter ratio of Asian dust observed with high-spectral resolution lidar and Raman Lidar, Appl. Optics, 41, 2760. https://doi.org/10.1364/AO.41.002760, 2002.

Lu, M.,Yang, X., Zhao, T., He, Q., Lu, H., Mamtimin, A., Huo, W., Yang, F., Liu, C., 2018. Modeling study on three-dimensional distribution of dust aerosols during a dust storm over the Tarim Basin, Northwest China. Atmospheric Research, 218(2019): 285-295.

Luo, C., W. Wang, L. Sheng, Y. Zhou, Z. Hu, W. Qu, X. Li and S. Hai, 2020: “Influence of polluted dust on chlorophyll-a concentration and particulate organic carbon in the subarctic North Pacific Ocean based on satellite observation and the WRF-Chem simulation”, *Atmos. Res.*, **236**, 104812. https://doi.org/10.1016/j.atmosres.2019.104812.

Ma, X., Bartlett, K., Harmon, K., Yu, Y., 2013.Comparison of AOD between CALIPSO and MODIS: significant differences over major dust and biomass burning regions. Atmospheric Measurement Techniques 6(9), 2391-2401.

Mace, G.G., Zhang, Q., Vaughan, M., Marchand, R., Stephens, G., Trepte, C., Winker, D., 2009. A description of hydrometeor layer occurrence statistics derived from the first year of merged CloudSat and CALIPSO data. J. Geophys. Res. Atmos., 114(D8).

Mahowald, N. M., Engelstaedter, S., Luo, C., Sealy, A., Artaxo, P., Benitez-Nelson,C., Bonnet, S., Chen, Y., Chuang, P. Y., Cohen, D. D., Dulac, F., Herut, B., Johansen, A. M., Kubilay, N., Losno, R., Maenhaut, W., Paytan, A., Prospero, J. M., Shank, L. M., and Siefert, R. L.: Atmospheric iron deposition: global distribution, variability, and human perturbations, Annu. Rev. Mar. Sci., 1, 245–278. https://doi.org/10.1146/annurev.marine.010908.163727, 2009.

Mbourou G N T, Bertrand J J, Nicholson S E. The diurnal and seasonal cycles of wind-borne dust over Africa north of the equator. Journal of Applied Meteorology, 1997, 36(7): 868-882.

Mehta, M., Singh, N., Anshumali. Global trends of columnar and vertically distributed properties of aerosols with emphasis on dust, polluted dust, and smoke - inferences from 10-year long CALIOP observations. Remote Sensing of Environment 2018, 120-132.

Ming H, Wei M, Wang M. Quantitative Detection of Dust Storms with the Millimeter Wave Radar in the Taklimakan Desert. Atmosphere, 2019, 10(9): 511.

Nan Y , Wang Y . De-coupling interannual variations of vertical dust extinction over the Taklimakan Desert during 2007–2016 using CALIOP. Science of The Total Environment, 2018, 633:608-617.

Pan H, Wang M, Kumar K R, et al. Seasonal and vertical distributions of aerosol type extinction coefficients with an emphasis on the impact of dust aerosol on the microphysical properties of cirrus over the Taklimakan Desert in Northwest China. Atmospheric Environment, 2019, 203: 216-227.

Pan, H., Bu, L., Kumar, K.R., Gao, H., Huang, X., Zhang, W. A new retrieval method for the ice water content of cirrus using data from the CloudSat and CALIPSO. J. Atmos. Solar-Terrest. Phys., 2017, 134-142.

Proestakis, E., Amiridis, V., Marinou, E., Georgoulias, A. K., Solomos,S., Kazadzis, S., Chimot, J., Che, H., Alexandri, G., Binietoglou,I., Daskalopoulou, V.,Kourtidis, K. A., de Leeuw,G., and van der A, R. J.: Nine-year spatial and temporal evolution of desert dust aerosols over South and East Asia as revealed by CALIOP, Atmos. Chem. Phys., 18, 1337–1362. https://doi.org/10.5194/acp-18-1337-2018, 2018.

Rosenfeld, D., Lohmann, U., Raga, G. B., O’Dowd, C. D., Kulmala, M., Fuzzi, S., Reissell, A., and Andreae, M. O.: Flood or drought: how do aerosols affect precipitation?, Science, 321, 1309–1313, 2008.

Sakai, T., Nagai, T., Nakazawa, M., and Matsumura, T.: Ramanlidar measurement of water vapor and ice clouds associated withAsian dust layer over Tsukuba, Japan, Geophys. Res. Lett., 31, L06128, doi:10.1029/2003GL019332, 2004.

Sassen, K., DeMott, P. J., Prospero, J. M., and Poellot, M.R.: Saharan dust storms and indirect aerosol effect on clouds:CRYSTAL-FACE results, Geophys. Res. Lett., 30(12), 1633, doi:10.1029/2003GL017371, 2003.

Shao, Y., Klose, M., and Wyrwoll, K.: Recent global dust trend and connections to climate forcing, J. Geophys. Res., 118, 11107–11118. https://doi.org/10.1002/jgrd.50836, 2013.

Shao, Y., Wyrwoll, K., Chappell, A., Huang, J., Lin, Z., McTainsh, G., Mikami, M., Tanaka, T., Wang, X., and Yoon, S.: Dust cycle: an emerging core theme in Earth system science, Aeolian Res., 2, 181–204. https://doi.org/10.1016/j.aeolia.2011.02.001, 2011a.

Sheng et al., Atmospheric Physcis. Beijing: Peking University press, 2003:19-21.

Shikwambana, L., Sivakumar, V., 2018. Global distribution of aerosol optical depth in 2015 using CALIPSO level 3 data.Journal of Atmospheric and Solar-Terrestrial Physics.173. https://doi.org/10.1016/j.jastp.2018.04.003.

Smith, K. L. and Kushner, P. J., 2012. Linear interference and the initiation of 531 extratropical stratosphere-troposphere interactions. Journal of Geophysical 532 Research Atmospheres, 117(D13), doi: 10.1029/2012JD017587.

Stephens, G.L., Vane, D.G., Tanelli, S., Im, E., Durden, S., Rokey, M., Reinke, D., Partain, P., Mace, G.G., Austin, R., Ecuyer, T.L., Haynes, J., Suzuki, K., 2008.CloudSat mission: performance and early science after the first year of operation. J. Geophys. Res. Atmos. 113 (8), 2036–2044.

Sun, J., Zhang, M., Liu, T., 2001. Spatial and temporal characteristics of dust storms in China and its surrounding regions, 1960–1999: Relations to source area and climate. Journal of Geophysical Research Atmospheres. 106(D10), 10325–10334, 536, doi: 10.1029/2000JD900665.

Tanaka, T.Y., Chiba, M., 2006.A numerical study of the contributions of dust source regionsto the global dust budget. Glob.Planet.Chang. 52, 88–104.

Textor, C., Schulz,M., Guibert, S., Kinne, S., Balkanski, Y., Bauer, S., et al., 2006. Analysis and quantification of the diversities of aerosol life cycles within AeroCom. Atmos. Chem. Phys. 6, 1777–1813.

Tian, P., X. Cao, L. Zhang, N. Sun, L. Sun, T. Logan, J. Shi, Y. Wang, Y. Ji, Y. Lin, Z. Huang, T. Zhou, Y. Shi and R. Zhang, 2017: “Aerosol vertical distribution and optical properties over China from long-term satellite and ground-based remote sensing”, Atmos. Chem. Phys., 17, 2509-2523.

Twomey, S.; Piepgrass, M.;Wolfe, T. An assessment of the impact of pollution on global cloud albedo. Tellus B1984, 36, 356–366.

Uno, I., Eguchi, K., Yumimoto, K., Takemura, T., Shimizu, A., Uematsu, M., et al., 2009.Asiandust transported one full circuit around the globe. Nat. Geosci. 2, 557–560.

Vaughan, M., A. Garnier, D. Josset, M. Avery, K.-P. Lee, Z. Liu, W. Hunt, J. Pelon, Y. Hu, S. Burton, J. Hair, J. Tackett, B. Getzewich, J. Kar and S. Rodier, 2019: “CALIPSO Lidar Calibration at 1064 nm: Version 4 Algorithm”, Atmos. Meas. Tech., 12, 51-82. https://doi.org/10.5194/amt-12-51-2019.

Wang, M., Wei, W., He, Q., Yang, Y., Fan, L., Zhang, J., 2016. Summer atmospheric boundary layer structure in the hinterland of Taklimakan Desert, China. Journal of Arid Land, 8(06):846-860, doi: 10.1007/s40333-016-0054.

Winker, D. M., Hunt, W. H., and McGill, M. J., 2007. Initial performance assessment of CALIOP, Geophys. Res. Lett., 34, L19803. https://doi.org/10.1029/2007GL030135.

Winker, D.M., Vaughan, M., Omar, A.H., Hu, Y., Powell, K.A., Liu, Z., Hunt, W.H., Young, S.A., 2009. Overview of the CALIPSO Mission and CALIOP data processing algorithms. J. Atmos. Ocean. Technol. 26 (11), 2310–2323.

Yang X, Shen S, Yang F, et al. Spatial and temporal variations of blowing dust events in the Taklimakan Desert. Theoretical and applied climatology, 2016, 125(3-4): 669-677.

Yang, F., Huang, J., Zhou, C., Yang, X., Ali, M., Li, C., et al. 2020. Taklimakan desert carbon-sink decreases under climate change. Science Bulletin, 65(6), 431–433, doi:10.1016/j.scib.2019.12.022

Yumimoto, K., Eguchi, K., Uno, I., Takemura, T., Liu, Z., Shimizu, A., Sugimoto, N. An elevated large-scale dust veil from the Taklimakan desert: intercontinental transport and three-dimensional structure as captured by CALIPSO and regional and global models. Atmospheric Chemistry and Physics Discussions, 2009, 9(4), 8545-8558.

Zeng, Z.-C., S. Chen, V. Natraj, T. Le, F. Xu, A. Merrelli, D. Crisp, S. P. Sander and Y. L. Yung, 2020: “Constraining the vertical distribution of coastal dust aerosol using OCO-2 O2 A-band measurements”, *Remote Sens. Environ.*, **236**, 111494. https://doi.org/10.1016/j.rse.2019.111494.

Zhang X., Sharratt B., Liu L., et al., 2019. East Asian dust storm in May 2017: observations, modelling,and its influence on the Asia-Pacific region. Atmos. Chem. Phys. https://doi.org/10.5194/acp-18-8353-2018.

Zhou C, Mamtimin A , Yang F, et al. Dust uplift potential in the Taklimakan Desert: an analysis based on different wind speed measurement intervals. Theoretical and Applied Climatology, 2018.

Table 1. The CALIPSO overpass time over the TD area and the observed radiosonde sounding time at Tazhong site.

Sounding Station (°N,°E)	Radiosonde Sounding Time (YYYY-MM-DD-hh:mm/UTC)	CALIPSO overpass coordinates over the TD (°N)(°E)	CALIPSO overpass time range (YYYY-MM-DD-hh:mm:ss/UTC) over the TD	Time interval (or difference) between sounding and satellite detection. (hh: mm)
Tazhong (39.04,83.63)	2016-07-01-06:00	(37.02,40.98) (80.80,79.5)	2016-07-01-07:56:21-07:57:27	01:57
	2016-07-02-18:00	(41.00,37.04) (83.35,82.13)	2016-07-02-20:39:33-20:40:39	02:40
	2016-07-03-06:00	(37.02,40.98) (83.90,82.68)	2016-07-03-07:43:56-07:45:02	01:45
	2016-07-04-18:00	(41.00,37.04) (86.44,85.23)	2016-07-04-20:27:09-20:28:14	02:28
	2016-07-05-06:00	(37.02,40.98) (87.00,85.78)	2016-07-05-07:31:31-07:32:37	01:32
	2016-07-07-18:00	(40.99,37.03) (78.74,77.51)	2016-07-07-20:57:59-20:59:05	02:59
	2016-07-08-06:00	(37.04,41.00) (79.27,78.05)	2016-07-08-08:02:24-08:03:30	02:03
	2016-07-09-18:00	(40.96,37.04) (81.81,80.60)	2016-07-09-20:45:40-20:46:46	02:46
	2016-07-10-06:00	(37.03,40.99) (82.36,81.13)	2016-07-10-07:50:04-07:51:10	01:51
	2016-07-11-18:00	(40.96,37.04) (84.89,83.68)	2016-07-11-20:33:20-20:34:26	02:34
	2016-07-12-06:00	(37.03,40.99) (85.44,84.21)	2016-07-12-07:37:44-07:38:51	01:38
	2016-07-13-18:00	(40.99,37.03) (87.98,86.76)	2016-07-13-20:21:00-20:22:06	02:22
	2016-07-14-06:00	(37.04,40.96) (88.51,87.30)	2016-07-14-07:25:25-07:26:30	01:26
	2016-07-16-18:00	(40.99,37.03) (80.24,79.02)	2016-07-16-20:51:56-20:53:03	02:53
	2016-07-17-06:00	(37.00,40.96) (80.79,79.56)	2016-07-17-07:56:20-07:57:27	01:57
	2016-07-18-18:00	(40.96,37.00) (83.31,82.09)	2016-07-18-20:39:37-20:40:43	02:40

2016-07-19-06:00	(37.03-41.00) (83.86,82.63)	2016-07-19-07:44-01-07:45:07	01:45
2016-07-20-18:00	(40.96,37.00) (86.40,85.17)	2016-07-20-20:27:16-20:28:23	02:28
2016-07-21-06:00	(37.03,40.99) (86.94,85.72)	2016-07-21-07:31:40-07:32:47	01:32
2016-07-23-18:00	(40.96,37.04) (78.66,77.45)	2016-07-23-20:58:12-20:59:18	02:59
2016-07-24-06:00	(37.04,40.96) (79.20,77.99)	2016-07-24-08:02:37-08:03:42	02:03
2016-07-25-18:00	(40.98,37.02) (81.75,80.52)	2016-07-25-20:45:51-20:46:58	02:46
2016-07-26-06:00	(37.02,40.98) (82.29,81.07)	2016-07-26-07:50:16-07:51:22	01:51
2016-07-27-18:00	(41.00,37.04) (84.84,83.61)	2016-07-27-20:33:31-20:34:37	02:34
2016-07-28-06:00	(37.01,40.97) (85.38,84.16)	2016-07-28-07:37:55-07:39:01	01:39
2016-07-29-18:00	(40.96,37.04) (87.91,86.70)	2016-07-29-20:21:11-20:22:16	02:22
2016-07-30-06:00	(37.00-40.96) (88.47,87.24)	2016-07-30-07:25:34-07:26:40	01:26

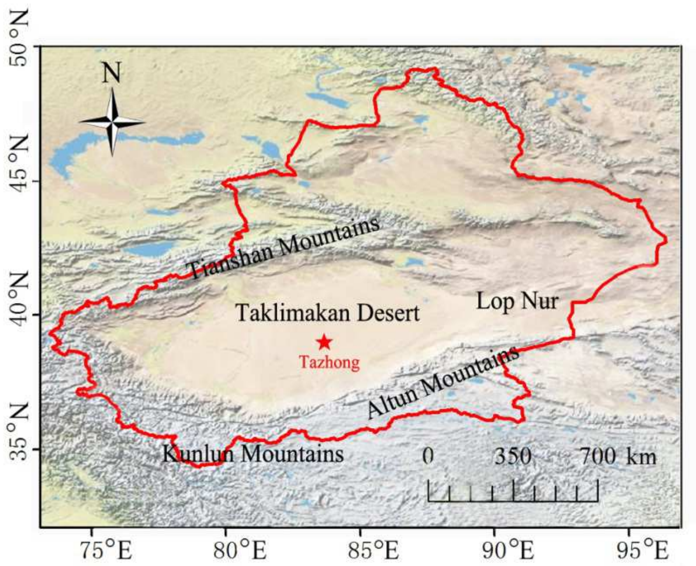

Fig. 1. Topography of the Taklimakan Desert (Source: Zhou et al., 2018).

Fig. 2. Trajectory map of CALIPSO transit over the Taklimakan Desert for July 1–30, 2016 (except July 6, 15, 22). (Web site: https://search.earthdata.nasa.gov)

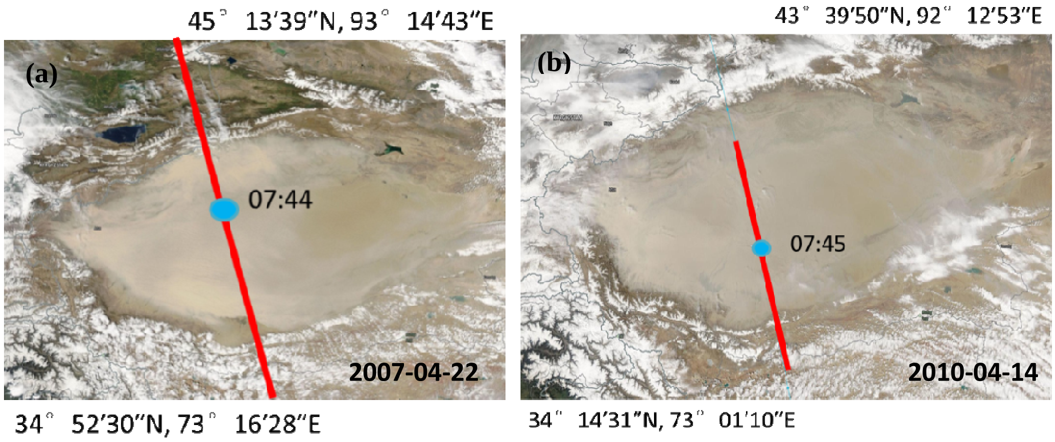

Fig. 3. True-color images derived from the MODIS Aqua over the TD for the selected two days representing strong DSs, April 22, 2007(a) and April 14, 2010(b). Satellite trajectories overpassing the TD and times (UTC) are presented by red lines and blue dots, respectively. Detailed content can be seen at the link: https://lance-modis.eosdis.nasa.gov/cgi-bin/imagery/gallery.cgi.

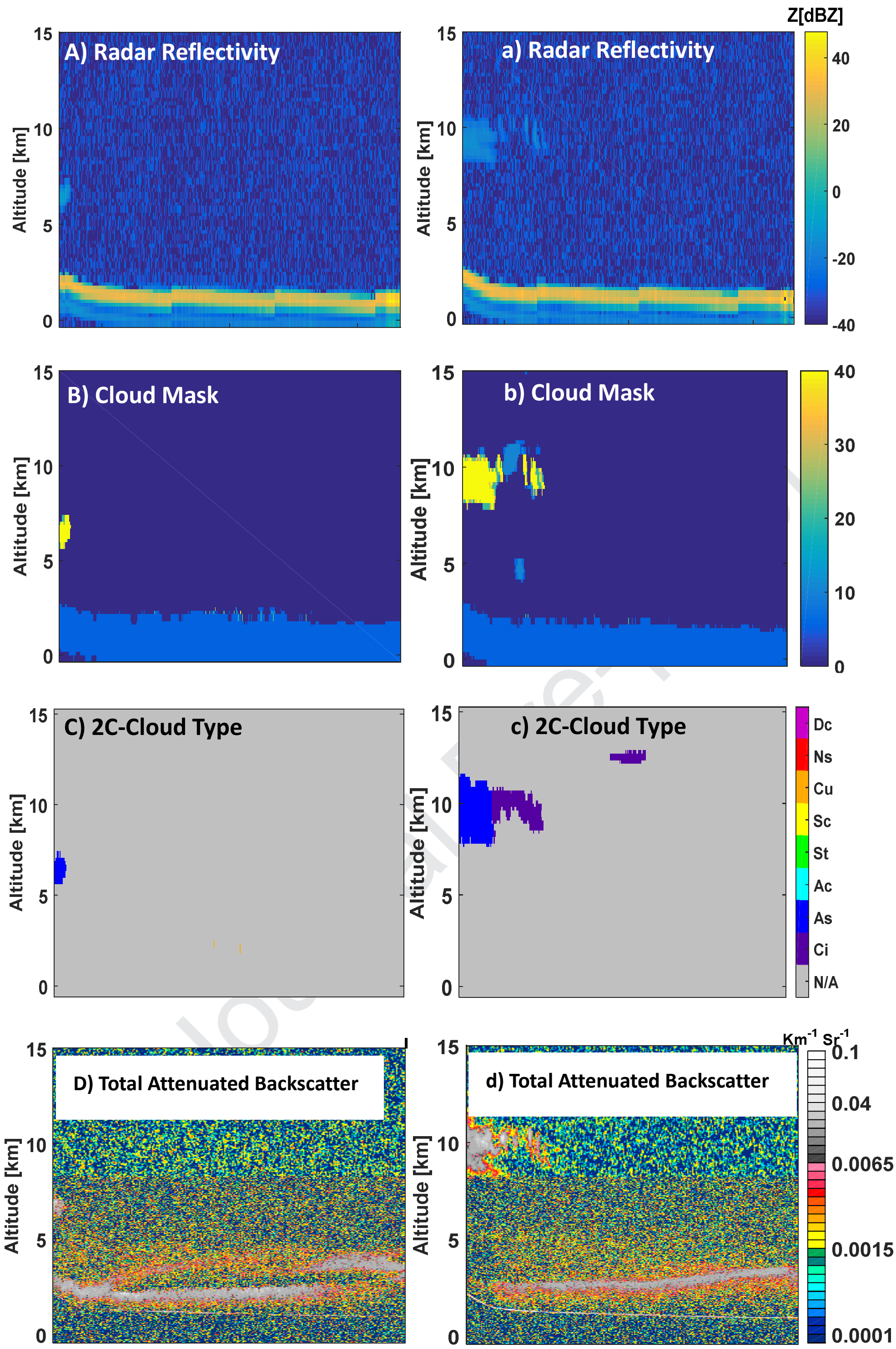

Fig. 4. The CALIPSO and CloudSat derived features for two typical strong DS events observed on 2007-04-22T07-12-34ZD-07:44:21-07:45:26 UTC (left A–H) and 2010-04-14T07-13-27ZD-07:45:55-07:47:02 UTC (right a–h) over the TD. (A-a) CloudSat radar reflectivity; (B-b) CloudSat cloud mask; (C-c) CloudSat and CALIPSO (2C) cloud type; (D-d) CALIPSO total attenuated backscatter; (E-e) CALIPSO vertical feature mask type; (F-f) CALIPSO aerosol type; (G-g) CALIPSO attenuated depolarization ratio; (H-h) CALIPSO attenuated color ratio.

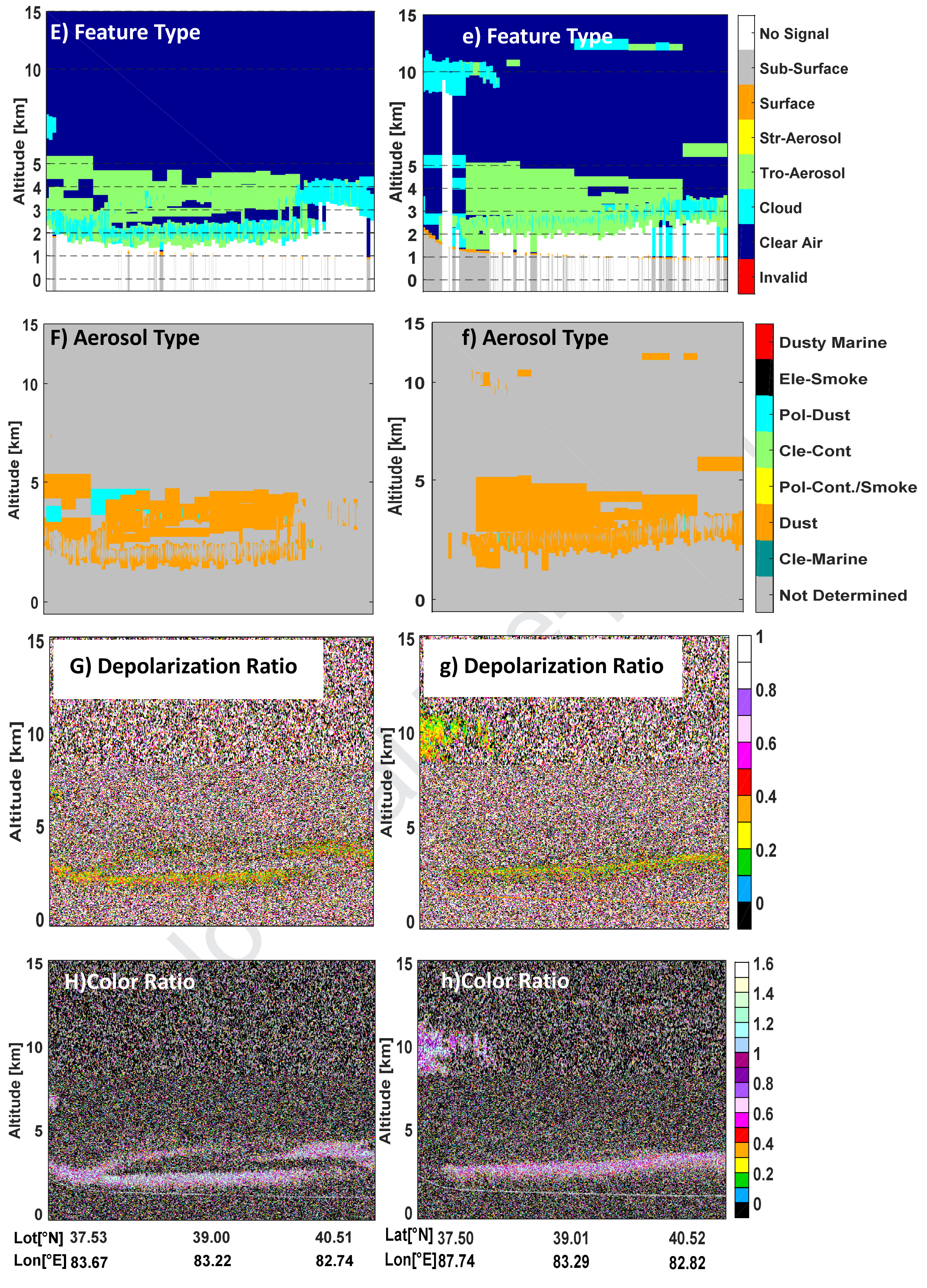

Fig. 4. (Continued).

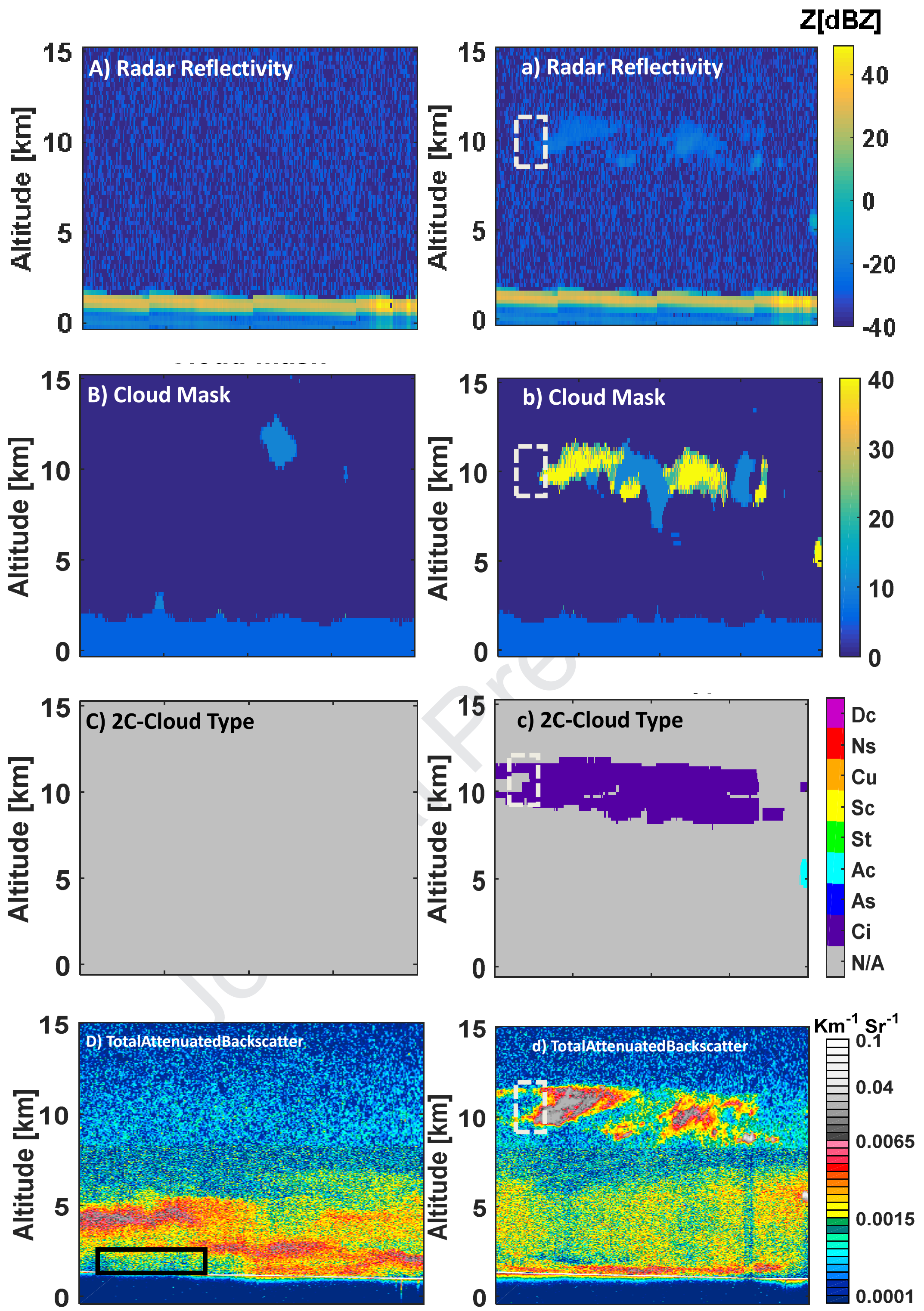

Fig. 5. Same as in Fig. 4, but for the CALIPSO and CloudSat derived features for two typical BD/FD events observed on 2007-05-14T20-40-56ZN-20:46:10-20:47:17 UTC (left A–H) and 2008-05-16T20-41-09ZN-20:46:08-20:47:14 UTC (right a–h) over the TD area.

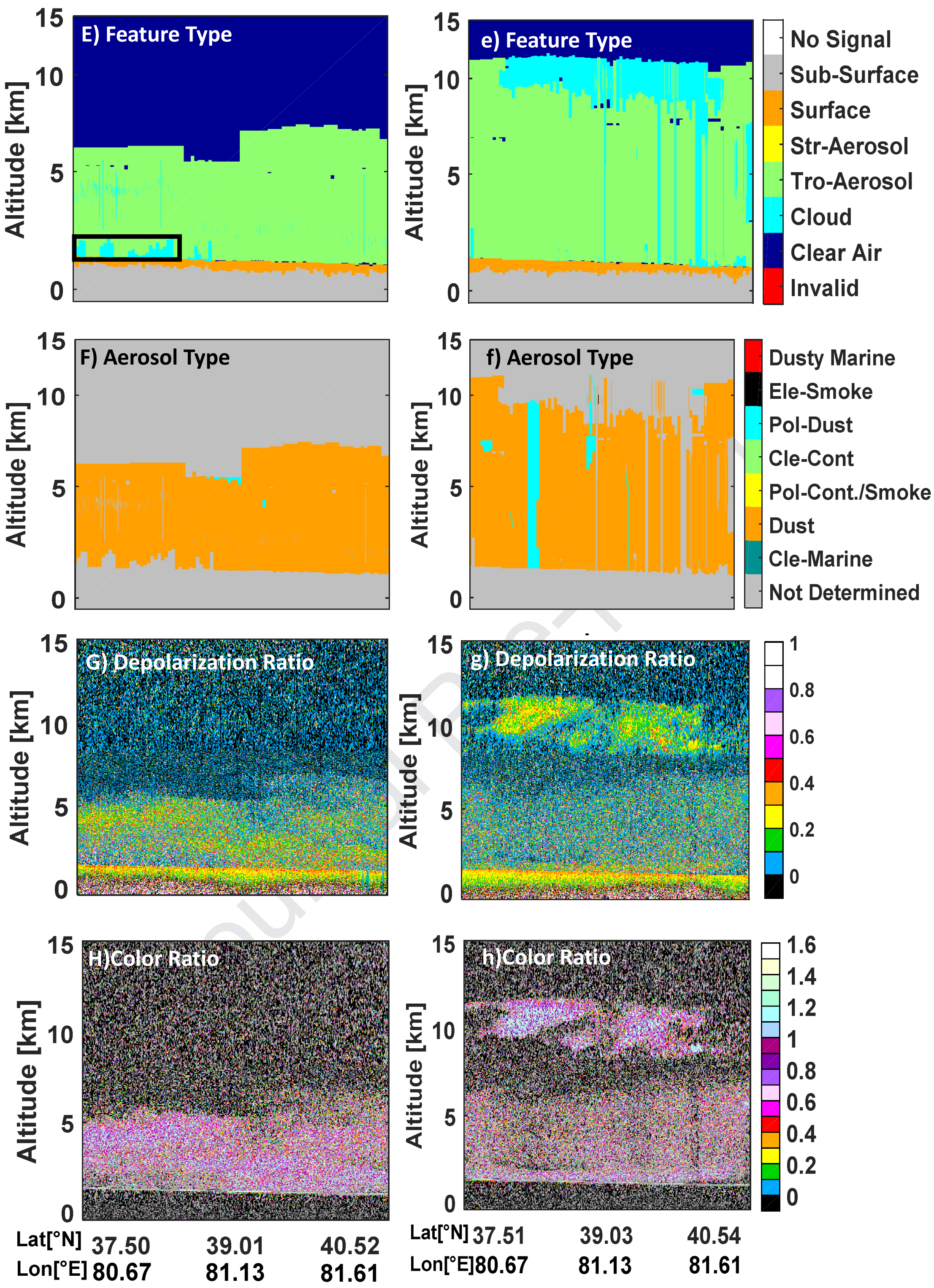

Fig. 5. (Continued).

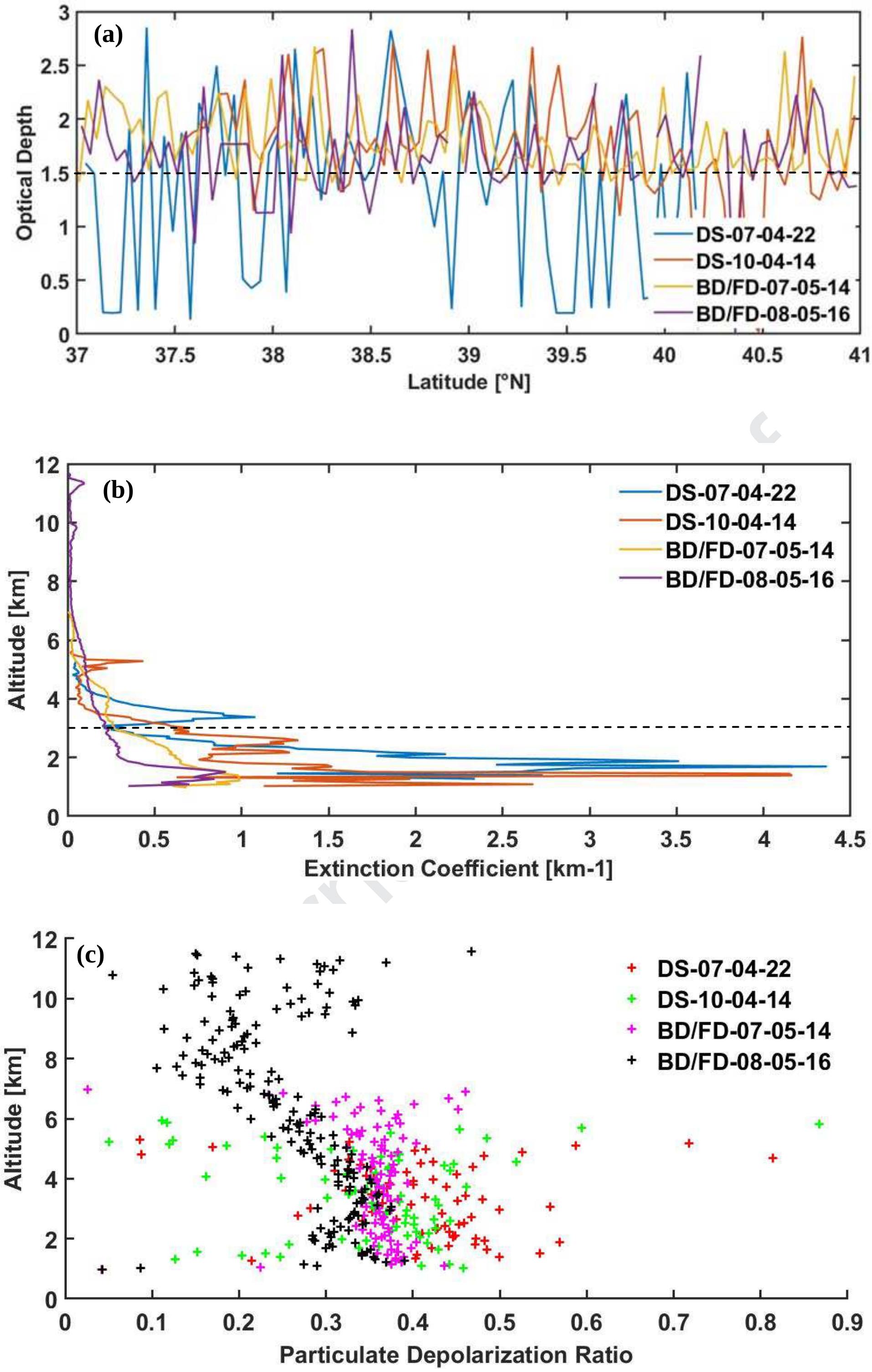

Fig. 6. Optical properties of sand-dust aerosol types (DS, BD/FD) for six typical cases. (a) Optical Depth for DS and BD/FD; (b) Mean Extinction Coefficient; (c) Mean Depolarization Radio; (d) Depolarization Radio. The labels in the panels indicate 20YY-MM-DD for the dust events (dust storm (DS), floating dust (FD), and blowing dust (BD)).

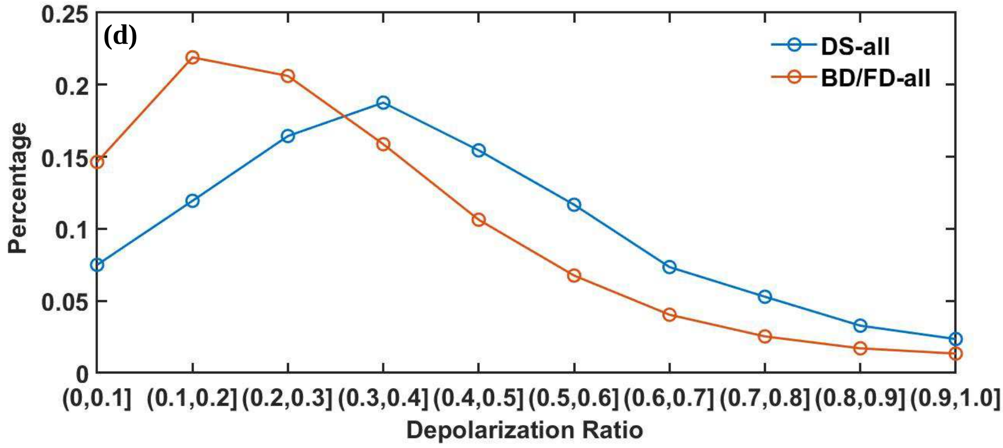

Fig. 6. (Continued).

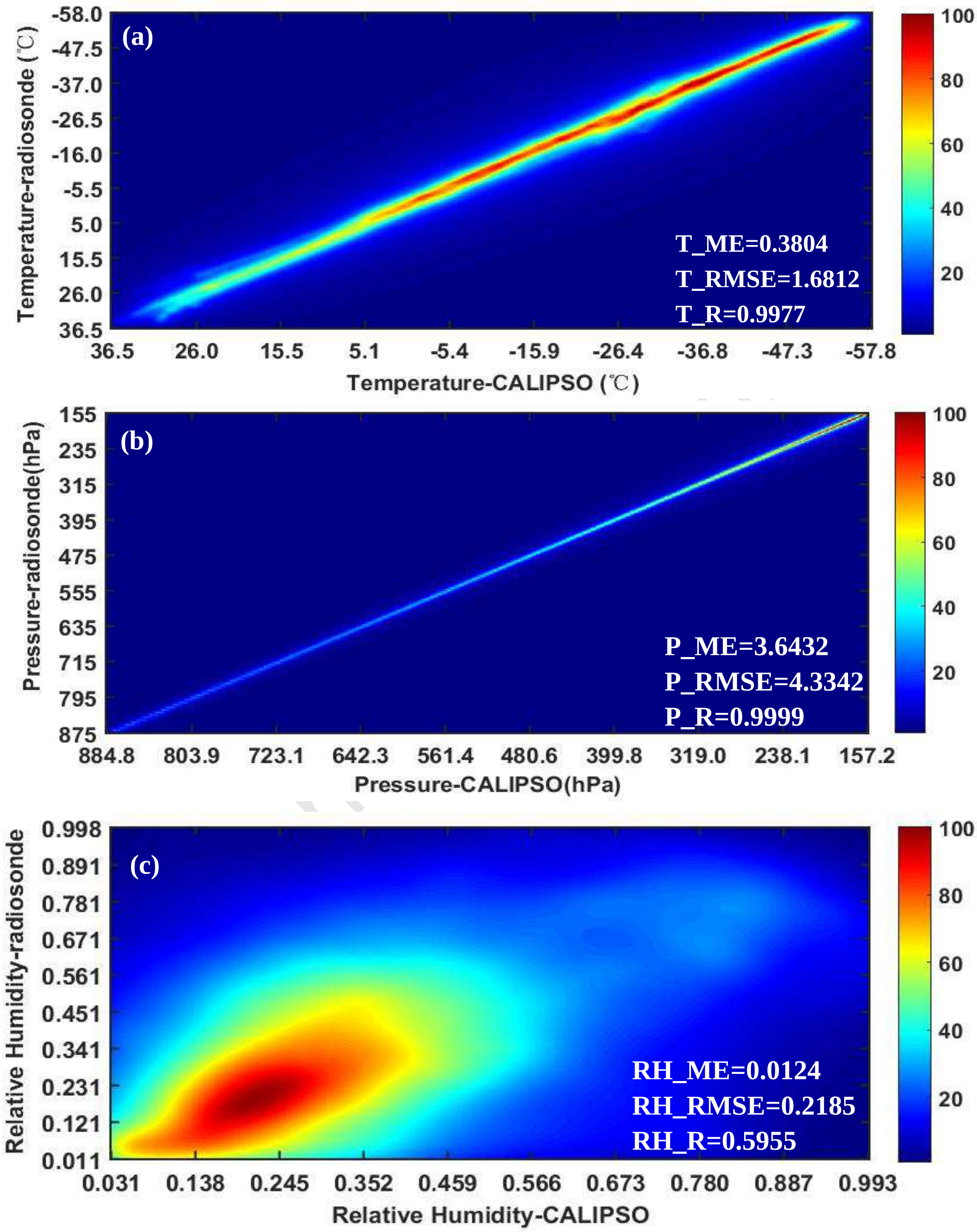

Fig. 7. The distribution of contour density plots between CALIPSO product and radiosonde sounding observation data. The color scale indicates the density of data points. (a) Temperature (T, □), (b) Pressure (P, hPa), (c) Relative Humidity (RH). (ME-mean error; RMSE- root mean square error; R- correlation coefficients)

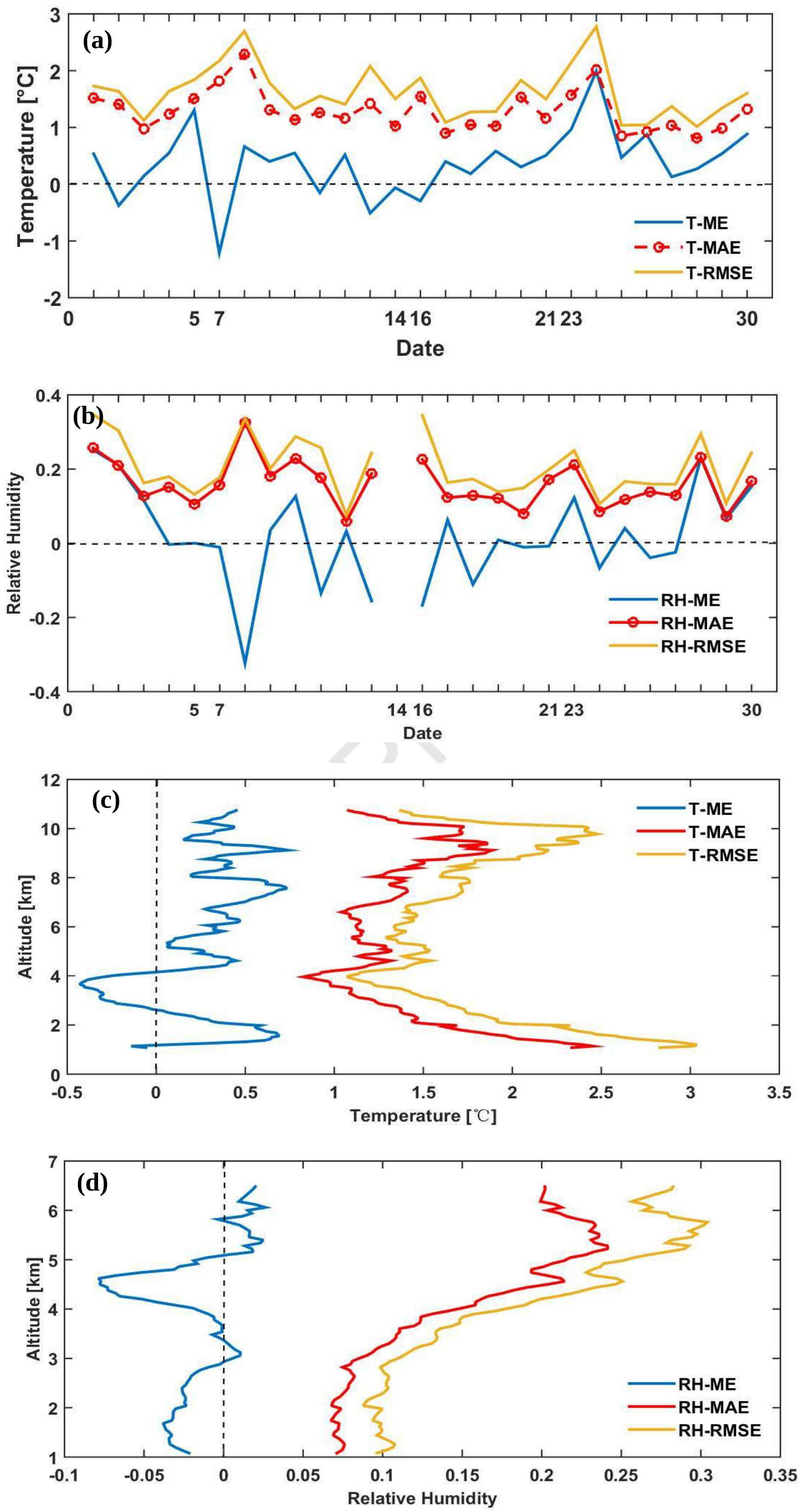

Fig. 8. The vertical profiles of ME, MAE, and RMSE of (a) Temperature (□) and (b) Relative Humidity observed from the CALIPSO product verified against the radiosonde data during the study period.

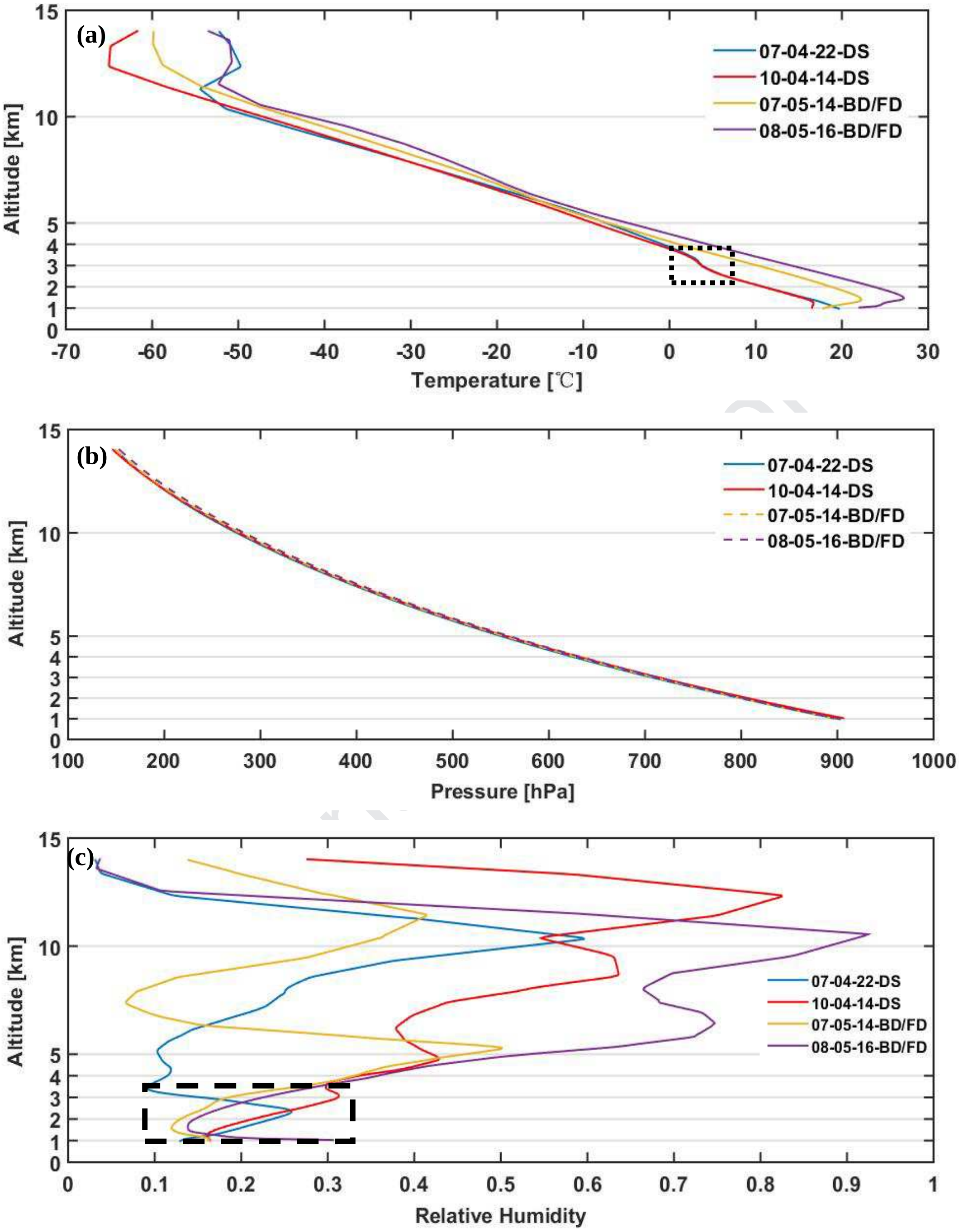

Fig. 9. Vertical profiles of temperature, pressure, and relative humidity obtained from the CALIPSO products in different densities of SDA types observed over the TD area. The labels indicate 20YY-MM-DD for the dust events (DS-dust strom; FD-floating dust; BD-blowing dust).

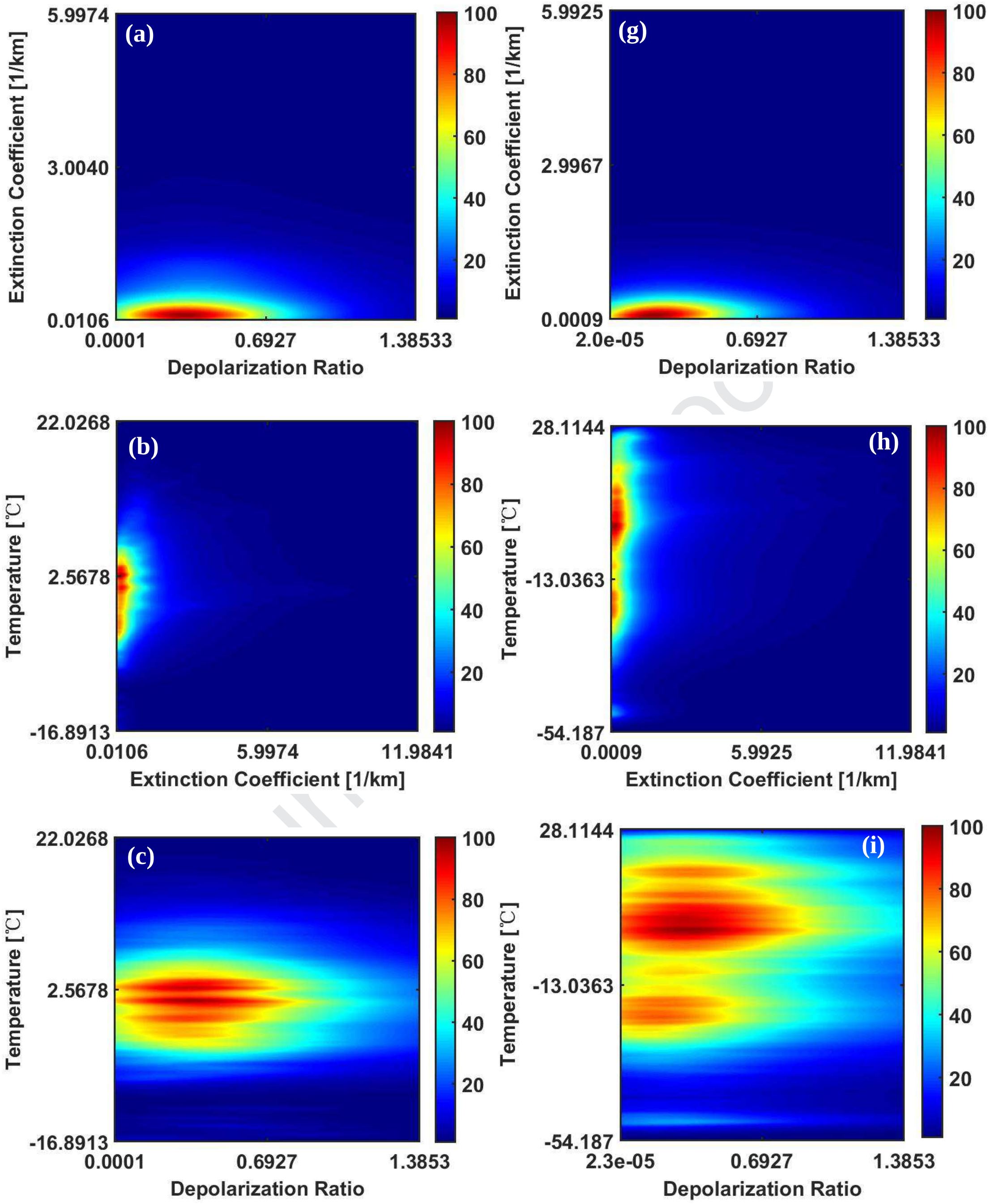

Fig. 10. Distribution of contour density plots between optical properties of SDAs and meteorological factors. The color scale indicates the density of data points (left-DS-all, right-BD/FD-all).

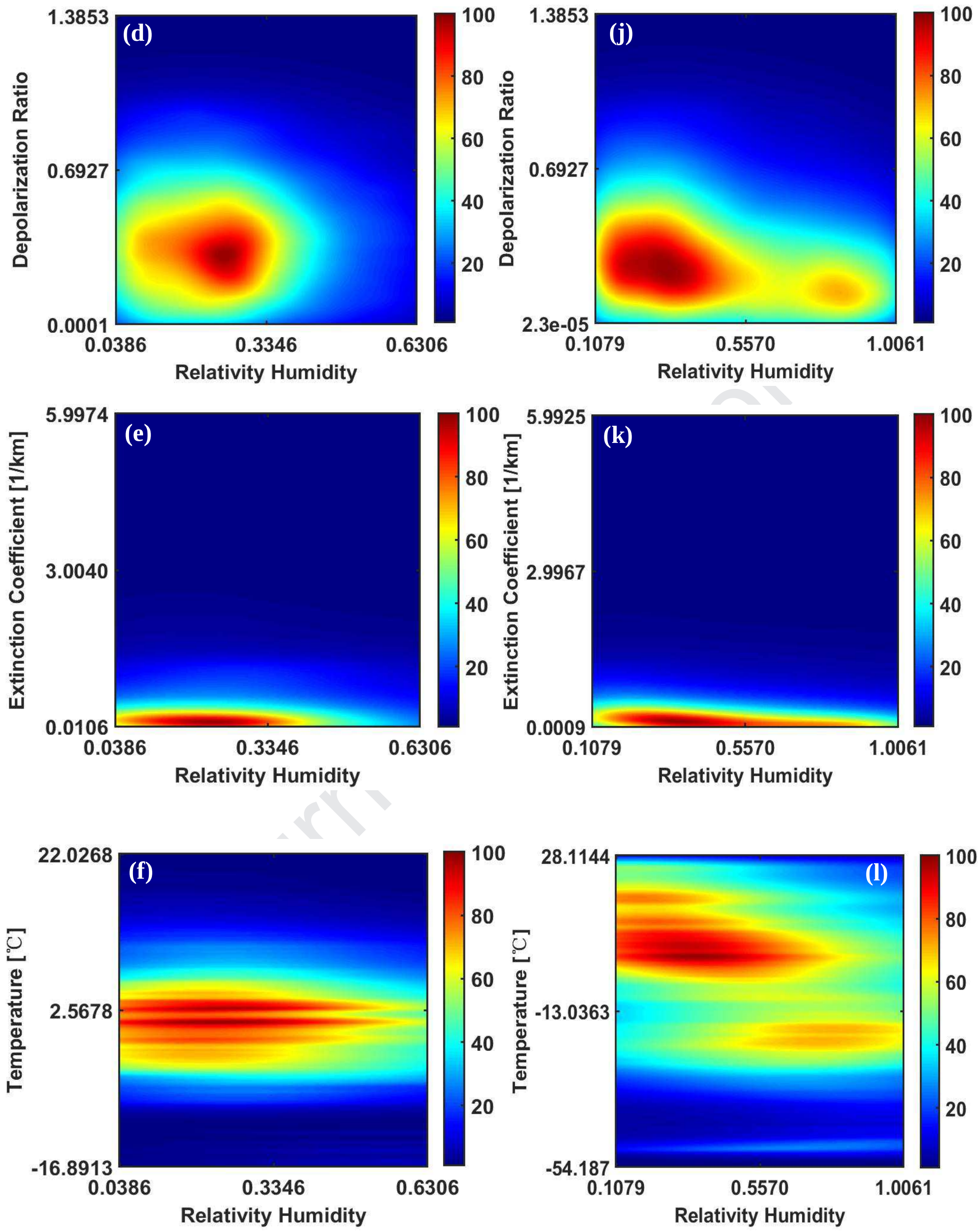

Fig. 10. (Continued).

Research Highlights

- We have investigated the optical properties of sand dust aerosols (SDAs) over the Taklimakan Desert from radiosonde and A-train satellite datasets.
- We have evaluated the correlation between SDAs and meteorological factors during spring.
- The meteorological factors observed from the CALIPSO are verified using the radiosonde data.

Statement of Declaration

The authors declare that we don't have any competing interest with the present study.